Università degli Studi di Padova
Dipartimento di Biologia
Corso di Laurea Magistrale in Biotecnologie Industriali

UItrastable Silver-Nanozymes surface-functionalized with artificial catalytic-triad biomimic esterase hydrolisis activity

Relatore: Prof. Alessandro Moretto
Dipartimento di Scienze Chimiche

Controrelatore: Prof.ssa Silvia Gross
Dipartimento di Scienze Chimiche

Laureanda: Varyzha Augustus A.

Anno Accademico 2022/2023

ABBREVIATIONS

Abbreviation	Correspondence
Ac O_2	Acetic anhydride
ACN	Acetonitrile
AcOEt	Ethyl acetate
Aib	α-aminoisobutyric acid
Boc	ter-butoxycarbonyl
DCC	N,N'-dicyclohexylcarbodiimide
DCM	Dichloromethane
DEC	N,N'-diisopropylcarbodiimide
DIPEA	N,N'-diisopropylethylamine
DMF	N,N-dimethylformamide
DMSO	Dimethyl sulfoxide
DODT	2,2-(Ethylenedioxy)diethanethiol
EDC*HCl	N-(3-dimethylaminopropyl)-N'-ethylcarbodiimide hydrochloride
EtOH	Ethanol
Fmoc	Fluorenylmethyloxycarbonyl
GSH	Glutathione
H NCH_{22} PhCl	4-Chlorobenzylamine
HATU	[Dimethylamino (triazolo [4,5-b] pyridin-3-yloxy) methylidene]-dimethylazanium; hexafluorophosphate
HOAt	1-Hydroxy-7-azabenzotriazole
HOBt	Hydroxybenzotriazole
HPLC	High-performance liquid chromatography
IR	Infrared
MeOH	Methanol
MM	Molar mass
NCA	N-carboxyanhydrides of α-amino acids.
NEt_3	Triethylamine
NHS	N-hydroxysuccinimide
NMR	Nuclear magnetic resonance imaging
NPs	Nanoparticles
pMBA	Para-mercaptobenzoic acid

ABSTRACT

Natural enzymes are essential catalysts for a wide range of reactions and they can have many applications in medicine, industry and research fields, but have some limitations such as sensitivity to environmental conditions, difficulty of isolation and lack of stability. The development of artificial catalysts represents a promising research field for catalysis. The use of nanomaterials offers many advantages, including the reduction of production costs, ease of large-scale production, increased stability, high surface reactivity and the ability to fine-tune the catalytic properties by changing the composition of the nanomaterial and of the linker used. In particular, enzyme-inspired catalytic nanosystems, also known as nanozymes, offer a promising alternative to traditional enzymes. Nanozymes based on metal nanoparticles surface functionalized with catalytic ligands may combine the stability and reproducibility of inorganic materials with the catalytic properties of the ligands composing the nanoparticles.

This research project focused on obtaining nanozymes with hydrolytic activity of ester substrates, exploiting highly stable silver nanoclusters functionalized with various artificial ligands inspired by the catalytic triad of esterases. Thiol-protected ultrastable silver nanoclusters were synthesized through chemical reduction. They were then functionalized with artificial catalytic-triad biomimetic peptides synthesized in solid phase. Several nanozyme candidates have been created, using different peptide ligands. Notably, one approach involved peptides containing the entire catalytic triad within a single unit, while another catalytic construct was designed by assembling two distinct helical peptides, each containing a part of the catalytic triad. Furthermore, nanozymes were enriched with alkyl chains to enhance their catalytic performance. Indeed, they create hydrophobic pockets, similar to those found in natural enzymes, to accommodate the catalytic residues, improving the catalytic efficiency of hydrolytic reactions on ester substrates and preventing the inactivation of the catalyst.

These nanozymes underwent to analysis of their physical and chemical properties, including the determination of the size and shape of the functionalized nanoclusters. Furthermore, the catalytic activity of the nanozymes was evaluated by specific tests using model ester substrates. Key factors influencing the catalytic performance,

such as nanozymes concentration, pH and reaction temperature, were investigated. Furthermore, the effect of hydrophobic environment on the catalytic performance of nanozymes was investigated, in order to optimize their selectivity and stability in an environment similar to that of native esterases. The kinetic results obtained by UV-visible spectrometry, which monitored the spectrum of the reaction product, demonstrated that the designed nanozymes exhibited high catalytic activity in ester conversion. This success suggests that such nanozymes may represent a promising alternative to natural esterases for ester hydrolysis, opening new perspectives for bio-catalytics and nanomedicine.

1. INTRODUCTION

1.1 Nanotechnologies

Nanoscience deals with the study of structures and molecules with dimensions ranging between 1 nm and 100 nm and while nanotechnology exploits these nanosystems in practical applications[1] . Nanotechnology is widely used in various economic sectors, and its impact on the market is becoming increasingly important, to such an extent that it is regarded by many experts as the next industrial revolution[2].

The increase in market value is certainly facilitated by the fact that nanotechnology is finding a wide range of applications in recent years. Many of these nanosystems are being exploited in the food, agricultural, cosmetics and chemical industries, but also in the medical, electronics and energy sectors[3].

The properties that benefit an object with dimensions in the nanoscale, the variety of substrates that can be exploited for synthesis, and the possibility of precisely controlling the shape and size of the nanosystem underpin their versatility[4].

1.2 Metal nanoparticles

Metal nanoparticles have peculiar properties, particularly their optical properties. These particles, consisting of metals such as gold, silver, platinum and copper, are in the nanometre range in size, resulting in a significant increase in their surface area relative to their volume. This phenomenon gives them unique optical characteristics, such as what is known as 'plasmonics', in which the electrons on the surface of the nanoparticle can collectively oscillate under the action of an electromagnetic field, giving rise to intensified optical absorption and scattering phenomena[5].

Gold and silver are the most used metals in nanotechnology due to their exceptional optical properties. Gold nanoparticles exhibit vivid colours that depend on the size

and shape of the particles, a phenomenon known as 'coloured colloid'. These unique optical properties make metal nanoparticles valuable in applications such as biosensors, cell labelling, biomedical imaging and photothermal therapy[6].

The optical properties of gold nanoparticles are defined by their plasmonic resonance band, which depends on both the collective state of electronic excitation and conduction and the structure, shape and size of the nanoparticles. The high molar absorption coefficient results in high selectivity, even higher than other chromophores, of optical detection techniques. Illuminating a solution of gold nanoparticles causes strong absorption and/or scattering at certain resonance wavelengths that depend largely on the morphology and dielectric constant of the medium[7].

A significant advantage of metal nanoparticles over other materials, especially in the catalytic field, is their high catalytic efficiency. The high ability to adsorb and activate reactive molecules on their surface allows metal nanoparticles to act as extremely active catalysts. Reactions catalysed by these nanoscale particles can take place at lower temperatures than conventional catalysts, thus reducing the energy required for the reaction[8].

Furthermore, the size and structure of metal nanoparticles can be modulated to optimise their catalytic activity for specific reactions, further improving process efficiency. By varying the reaction conditions, e.g. temperature, pH, reactant concentration, ionic strength, reaction time, solvent and type of stabilising agent and reducing agent, it is possible to obtain nanoparticles of different shapes and sizes[9].

1.3 Silver nanoparticles

Silver nanoparticles have attracted the interest of research mainly due to their optical properties (being endowed with an absorption spectrum usually characterised by a broad plasmonic band) and their efficient antibacterial and anticancer activities, making them excellent tools for medicine[10]. There are different methodologies for the synthesis of these nanoparticles, which are divided into chemical, physical and biological methods [Fig.1].

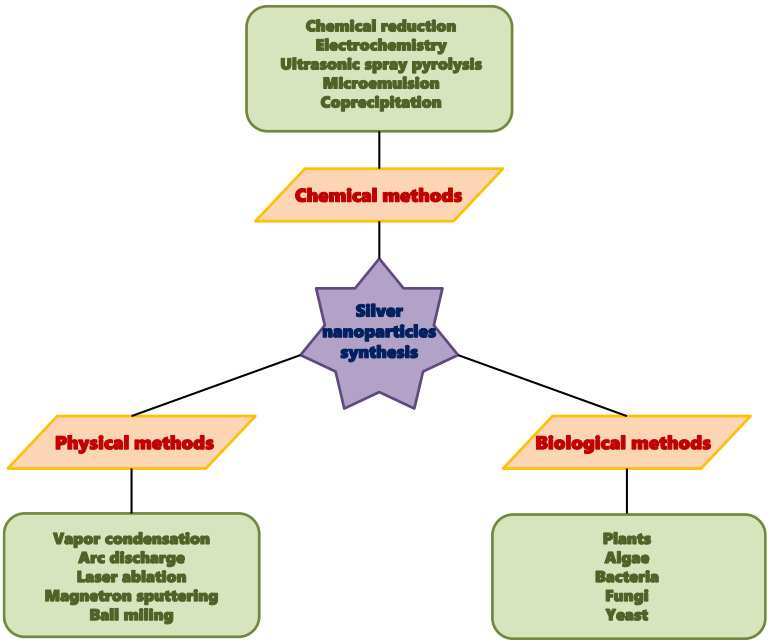

Fig.1 *Representation of some methodologies for the synthesis of silver nanoparticles.*

The most widely used methodology for the synthesis of silver nanoparticles exploits chemical reduction, in which the molecular players, as a general example, are the silver salt (typically $AgNO_3$) and the reducing agent $Ag^+ \rightarrow Ag^0$ (usually $NaBH_4$)[11].

1.3.1 Silver nanoparticles optical properties

Nanomaterials have different chemical/physical characteristics than bulk materials, since these depend heavily on the "surface area/volume" ratio. As the size decreases, the percentage of atoms on the surface in relation to the total number of atoms occupying a given volume increases, systematically affecting the characteristics of the object under consideration[12] . Metallic nanoparticles exhibit optical properties that are extremely sensitive to their shape, size, concentration and state of agglomeration, especially in the case of gold and silver nanoparticles, which interact strongly with precise wavelengths, making UV-VIS spectroscopy an excellent tool for the characterisation of these nanosystems[13]. In silver nanoparticles, the conduction and valence bands are close to each other, so the electrons are very free to move. If the material is irradiated with the appropriate

wavelength, this resonates with the conduction electrons, which give rise to a collective oscillation responsible for the characteristic absorption band called local surface plasmon resonance (LSPR)[14]. In one study, they identified how the different concentration of reducing agent used, in particular $NaBH_4$, resulted in colloidal nanoparticles of different colour, which is due to a different LSPR, in correlation with the variation in size and shape of the nanosystem [Fig.2][15] .

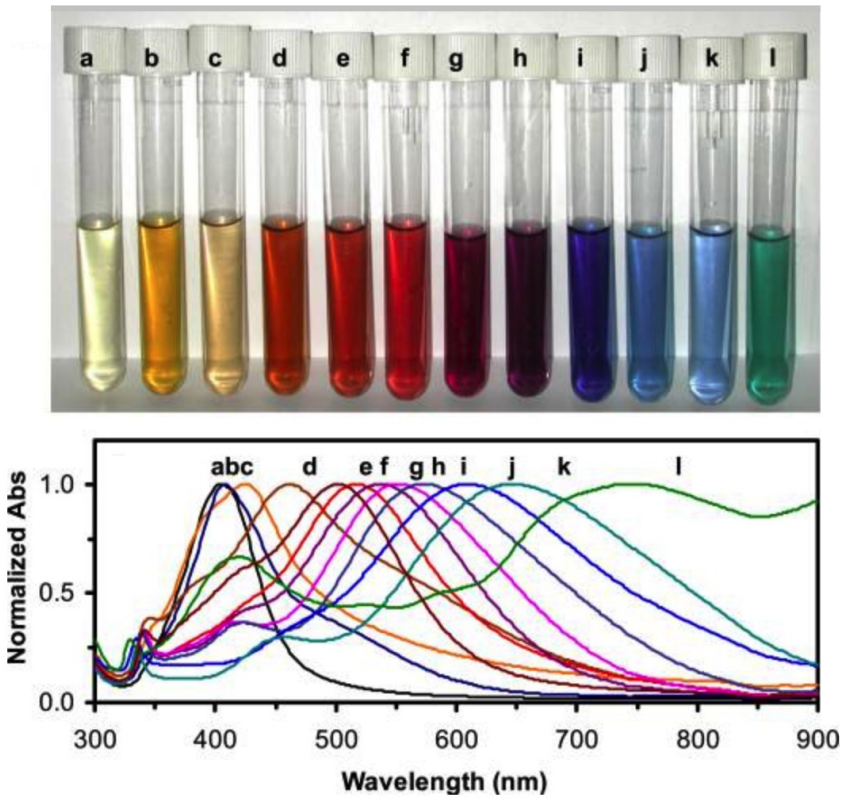

Fig.2 *Plasmonic absorption properties of different colloidal silver nanoparticles.*

1.3.2 Silver nanoparticles - Synthesis methodologies

Over the years, various methodologies have been adopted in the synthesis of silver nanoparticles; a distinction can be made between bottom-up approaches, in which the self-assembly of molecules in solution is exploited, and top-down approaches, in which the synthesis takes place from the bulk material. In addition to this distinction, the methodologies may be chemical or physical in nature.

1.3.2.1 Physical synthesis

Evaporation-condensation and laser ablation are the main physical techniques used. The former involves heating a solution of $AgNO_3$ and CH_3 COONa in a furnace, which is initially vaporised and after subsequent cooling, the desired nanoparticles are obtained. This method has disadvantages such as the high energy requirement and the excessive time required to achieve thermal stability[16].

The physical technique of laser ablation uses a laser pulsed at a precise wavelength, which is imprinted on the surface of the bulk material. The electric field generated is able to make free electrons oscillate on the surface of the material, which heats up and vaporises to become plasma, which can nucleate and form different nanostructures[17]. This method makes it possible to avoid contamination, and thanks to the possibility of varying process parameters, nanoparticles of different shapes and sizes can be obtained. When silver nanoparticles are intended to be used, for example, as an alternative to antibiotics in living organisms, it is essential that they do not contain any contamination or toxic substances from their synthesis[18].

Magnetron sputtering is another physical methodology used for the synthesis of silver nanoparticles. It exploits a sputtering gas that is first brought to a plasma state, forming extremely energetic particles, which are accelerated and used to bombard the bulk material, causing atoms to be released and deposited on a given substrate[19].

1.3.2.2 Chemical synthesis

The most widely used chemical synthesis exploits a reduction mechanism, in which the three molecular players, i.e. the silver salt, the reducing agent and the stabilising agent are used to control nanoparticle growth. Silver nitrate is commonly used as the salt due to its low cost and chemical stability. Sodium borohydride, citrate and ascorbate can be used as reducing agent, but the former allows rapid reduction and partially acts as a stabilising agent, preventing the aggregation of nanoparticles. As true stabilising molecules, polyvinylpyrrolidone (PVP), polyethylene glycol (PEG), polymethyl methacrylate (PMMA) and polymethacrylic acid (PMAA) are often

found, but heat-sensitive polymers such as poly(N-isopropylacrylamide) (PNIPAM) and collagenare also of interest[20]. An example of this synthesis methodology, in particular a co-reduction mechanism is exploited, shown in [Fig.3], where two reduction processes take place: the first operated by sodium borohydride and the second by trisodium citrate (TSC). The two reducing agents are mixed together for 30 min in the dark at 60°C, after which the silver salt is added drop by drop and the temperature is raised to 90°C, then basified with NaOH to pH 10.5. In the first nucleation step $NaBH_4$ performs the reduction $Ag^+ \rightarrow Ag^0$ resulting in the formation of the first silver nuclei that will participate in the growth process of the second stage in which the TSC acts. Eventually, the silver nanoparticles obtained are stabilised on their surface with negatively charged citrates, thus preventing aggregation[21].

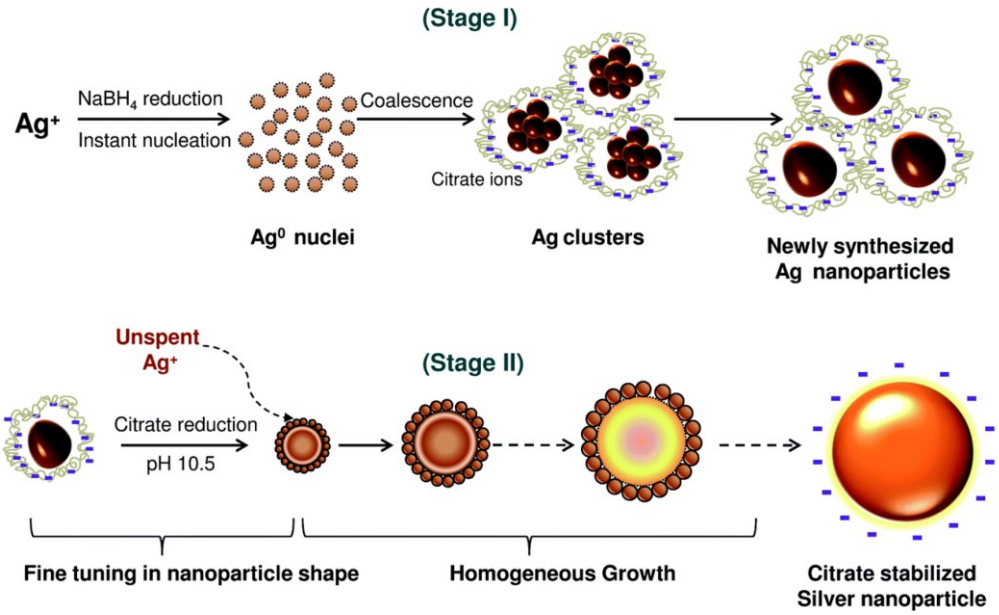

Fig.3 *Synthesis of silver nanoparticles using a co-reduction approach.*

A second chemical synthesis technique is the electrochemical method, in which the current density used can be varied to obtain nanoparticles of different shapes and sizes. In this methodology, as in the work of Roldán's group[22], a simple cell with two electrodes, both made of platinum, can be exploited. The reaction medium consists of the metal precursor, i.e. $AgNO_3$, and PEG, used as a stabilising agent.
One of the most innovative tools for chemical synthesis is ultrasonic spray pyrolysis (USP), a very powerful technique that makes it possible to conveniently obtain

nanoparticles with a narrow size distribution and purity. It starts with a dilute solution of the metal salt, which is first atomised to form an aerosol, then it enters the pyrolysis reactor at a temperature of around 650°C and finally the nanoparticles are deposited on the substrate of interest. The spray atomiser is connected to an ultrasonic generator and this allows the size of the aerosol droplets to be controlled, which is related to the morphology that the final nanostructures will have[23] .

1.4 Nanoparticles and nanoclusters

One of the main shortcomings of classic procedures for the synthesis of nanoparticles is that they fail to obtain unimolecular systems, since in the majority of cases a distribution in nanoparticle dimensions is obtained [Fig.4(A)]. Very often, the nanoparticles of interest carry ligands on their surface, i.e. organic molecules that can have various functions, from simple stabilisation of the system to the possibility of exploiting their properties in areas such as catalysis or diagnostics. The fact of having a polydispersion in size entails the problem of having nanoparticles composed of different, in number, metal atoms, thus also varying the amount of ligand present in each system. Furthermore, as the size of the nanoparticle increases, the surface of the nanoparticle appears flatter and flatter for ligand molecules. For example, if the ligand were a bioactive peptide, this would tend to adsorb and more easily cover the nanoparticle thanks to the interactions present between the orbitals of the amide bonds and those of the metal, in a process known as the 'corona effect', which causes the collapse of the peptide secondary structure and consequently the loss of its functionality [Fig.4(B)]. It is therefore clear how these aspects, in their synergy, clash with the idea of having a controlled, functional system with precise conformation.

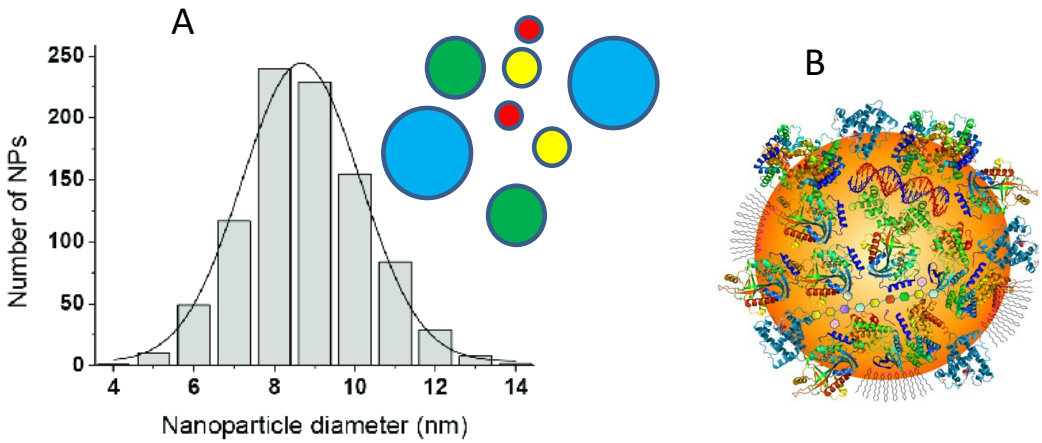

Fig.4 *Polydispersion in nanoparticle size following a classical chemical synthesis (A) and the 'corona effect' on a nanoparticle (B).*

Nanoclusters represent the optimal solution to the problems just described. Thanks to their properties, these systems are in the middle ground between well-defined molecules and plasmonic nanoparticles. Nanoclusters are in fact made up of precise combinations of metal atoms and organic ligands, which together lead to the formation of very small systems, where the diameter of the metal core usually does not exceed 2 nm. The smaller the size, the more the properties of nanoclusters tend to resemble those of small molecules, making them versatile molecular tools that can be used in various fields, including medicine and chemical catalysis. Among the variety of nanoclusters that can be synthesised, those formed as a result of the combination of metal atoms and thiol ligands are certainly the most studied. Examples of gold nanoclusters are shown in [Fig.5], in which one can see the precise spatial arrangement between the various atoms, which together define a very precise structure.

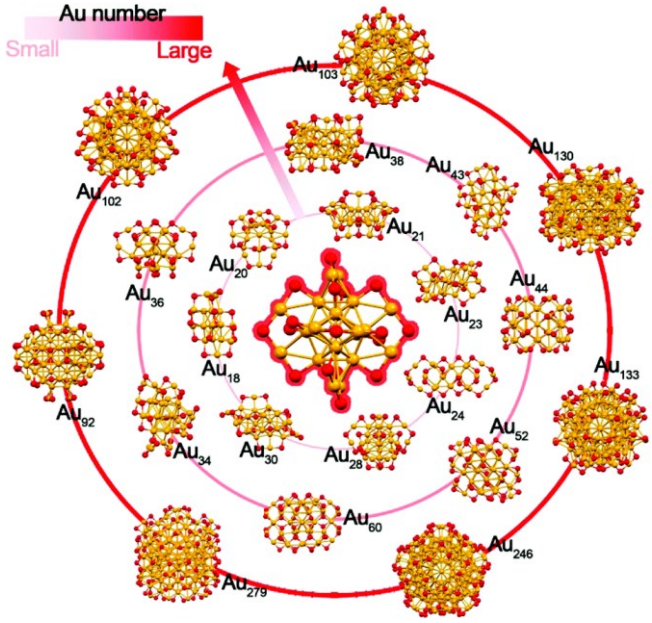

Fig.5 *Gold nanoclusters, examples of structures.*

1.4.1 Ultra-stable silver nanoclusters

In order to obtain a controllable system of precise composition, it is necessary to move from the world of plasmonic nanoparticles to that of nanoclusters. Desireddy et al.[(24)] has succeeded in obtaining silver systems that are truly characteristic for their structure and stability. They have synthesized silver clusters of precise composition, such that they can be associated with the molecular formula $M_4Ag_{44}(pMBA)_{30}$, thanks to protocol that simply involves the reduction with sodium borohydride of a semi-alkali solution of silver nitrate and the thiol ligand (para-mercaptobenzoic acid). The system has a very small size, with a metal core diameter of just 1.2 nm. Through X-ray crystallography analysis, the precise spatial arrangement of the silver atoms and ligand was obtained [Fig.6(B)], resulting in a complex yet compact structure, which together with the pMBA monolayer is responsible for the high stability of the nanoclusters. The small size and precise atomic composition make these systems true molecular entities, especially from the point of view of their optical properties, as they have a UV-VIS absorption spectrum characterised by several defined bands [Fig.6(A)] and not by a single plasmonic band characteristic of nanoparticles.

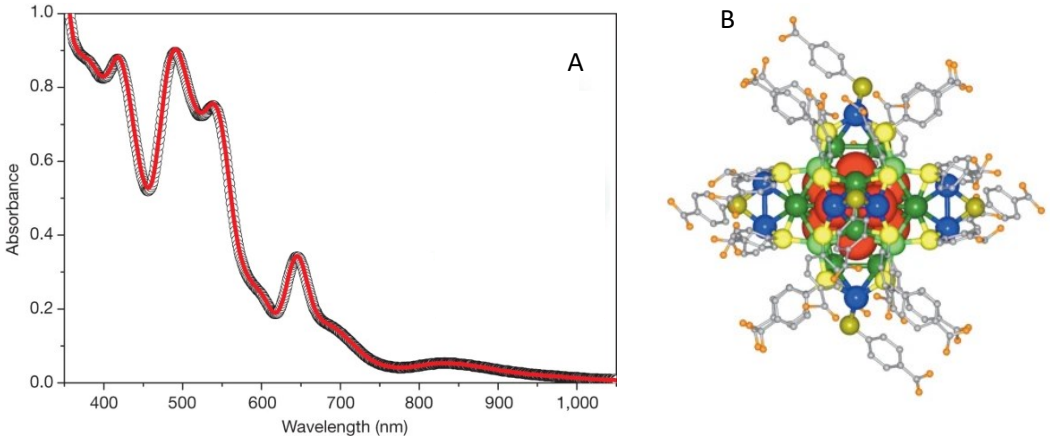

Fig.6 UV-VIS absorption spectrum of the nanocluster M_4 Ag_{44} $(pMBA)_{30}$ (A) and resolution of its molecular structure by X-ray crystallography (B).

1.4.2 Silver nanoclusters as enzyme-mimetic catalysts

Gold nanoclusters are used catalysts in various chemical reactions, e.g. the hydroamination of alkynes[25], the oxidation of alkenes[26], and the reduction of nitrate groups[27]. The nanoclusters synthesised by Desireddy's group offer an excellent basis for the realisation of more complex systems, but which base their strengths on the stability and easy preparation properties of the nanoclusters $M_4Ag_{44}(pMBA)_{30}$.

The aim of this thesis work is to synthesize silver nanoclusters that have catalytic properties towards ester bond hydrolysis, by engineering $M_4Ag_{44}(pMBA)_{30}$ nanoclusters. Esterases and proteases specialized in hydrolysis of the ester bond in their evolutionary pathway, optimising their three-dimensional conformation to efficiently carry out this type of reaction. Evolution has led to the formation of a highly conserved internal catalytic site in hydrolytic enzymes, which features the so-called 'catalytic triad', i.e. three residues (serine, histidine and aspartate) that cooperate in the catalysis of the ester/amide bond [Fig.7(A)]. The high enzymatic catalytic efficiency derives from: the catalytic triad, the chemical surroundings created within the enzyme pocket in which the substrate is to be placed and the

specific orientation between the catalytic residues which brings them into a certain spatial proximity.

This project aims to mimic the characteristics of the enzymatic catalytic site on the outer surface of nanoclusters, by exploiting particular peptide ligands derived from the functionalisation of pMBA [Fig.7(B)]. Within the enzyme pocket, the dielectric constant is lower due to the exclusion of water molecules, resulting in higher residue pKa values than under standard conditions, but which are essential for catalysis to take place.

Therefore, in the overall design of these enzyme-mimetic systems, the intention is to exploit the self-assembly of small peptides on the surface of the silver nanocluster, to recreate what is naturally present in the catalytic pocket of an enzyme.

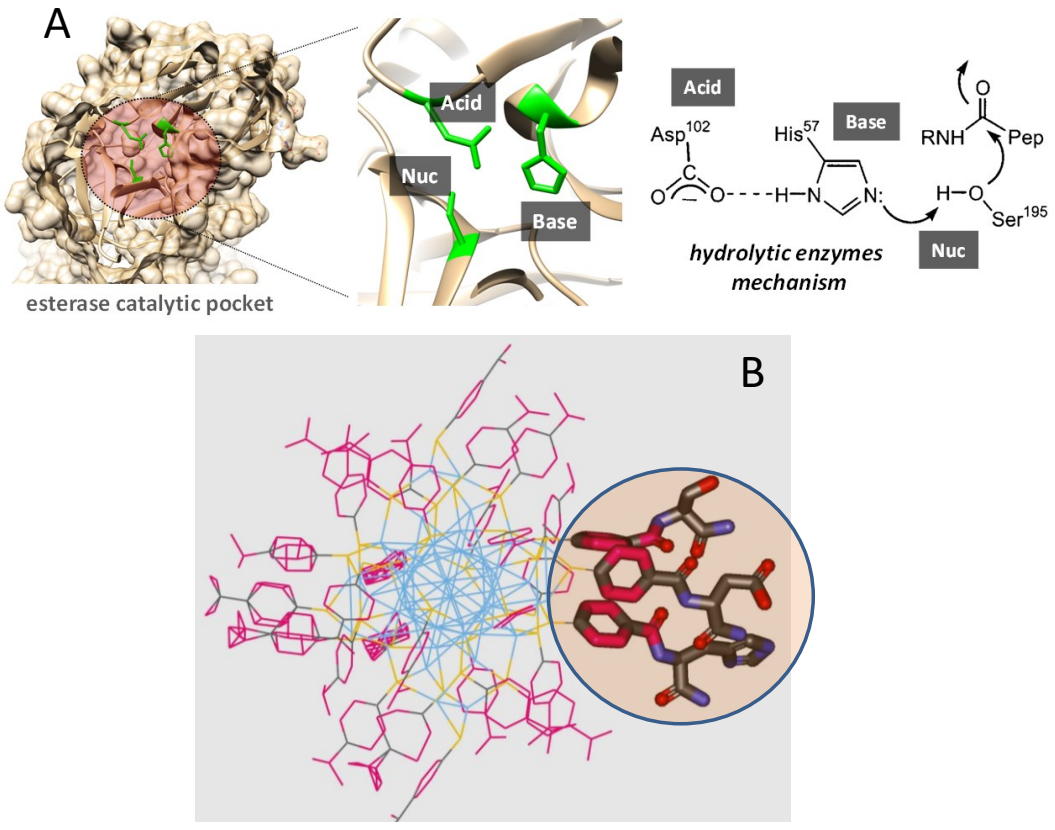

Fig.7 *Schematisation of the catalytic site of an esterase and the mechanism of hydrolytic catalysis against a peptide bond (A). In (B), the structure of the nanocluster* $M_4 Ag_{44} (pMBA)_{30}$ *and the pMBA ligand modified with small peptides is observed*

1.5 Hydrolysis of the ester bond

The ester hydrolysis reaction plays a crucial role in both biological and industrial fields. This reaction is responsible for the breakdown of esters within cells, releasing molecules needed for cell metabolism. In the industrial context, the ester hydrolysis reaction is used to produce various compounds, such as fatty acids, glycerol and other chemicals of commercial interest[28].

In the ester, the carbonyl carbon is depleted of electrons due to the proximity of the two oxygens, which, due to their higher electronegativity, tend to draw the bonding electrons towards them. This situation renders the carbonyl carbon electrophilic and can therefore be subject to nucleophilic attack reactions [Fig.8], in which a tetrahedral intermediate is passed through and an exiting group is expelled, leading to the formation of an alcohol (in the case of the nucleophile being H_2O) and a carboxylic acid or its salt. The hydrolysis reaction is kinetically unfavourable under standard conditions, so an acid- or base-catalysed procedure is usually followed. However, conditions of high acidity or basicity may cause discomfort to other molecular components in solution or other functional groups in the molecule itself, so strategies operating under mild conditions of temperature and pH are preferred.

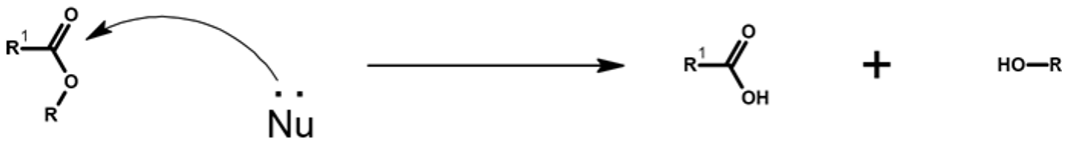

[Fig.8] *Representation of the nucleophilic attack on the carbonyl carbon of the ester, leading to the formation of carboxylic acid and alcohol.*

One alternative to chemical hydrolysis is enzymatic catalysis. Esterases and other related enzymes are responsible for catalysing these reactions in a highly specific and efficient manner. This has prompted the search for artificial catalysts that can emulate the functions of esterases and other enzymes involved in ester hydrolysis reactions[29].

However, there are cases where enzymes are not suitable for industrial needs or cannot be easily integrated into specific processes. Like all enzymes, their high

efficiency and selectivity can only be achieved by operating under the right conditions.

This is why in recent years, research has been focusing more and more on the synthesis of new catalysts defined as enzyme-mimetic, very often exploiting the principles of supramolecular chemistry to recreate in the system of interest what naturally occurs inside the enzymatic catalytic pocket.

The design of artificial catalysts represents a significant challenge, as it requires a detailed understanding of the chemical and structural interactions involved in enzymatic reactions. However, success in this field can lead to considerable benefits, such as the possibility of controlling and optimising specific chemical reactions, improving the efficiency of industrial processes and opening the way to new applications. The search for artificial catalysts inspired by biological enzymes not only contributes to industrial innovation, but also offers the opportunity to better understand the biological mechanisms and molecular interactions that drive natural enzyme catalysis[30].

1.5.1 Enzymatic hydrolysis

In their evolutionary course, enzymes have been selected for their selectivity (chemo-, regio- and enantio-selectivity) and for their high catalytic efficiency, which is far greater than that achievable with homogeneous and heterogeneous chemical catalysis.

Esterases are hydrolytic enzymes that act on breaking the ester bond and are proteins expressed by most organisms, playing an important role in various metabolic processes such as digestion, detoxification and anti-inflammatory mechanisms.

The interesting catalytic properties of enzymes derive from the protein's three-dimensional structure, leading to the formation of catalytic pockets in which the substrate is stabilised through specific non-covalent interactions with certain protein residues. The catalytic site has a good affinity for the substrate, but not too much; to obtain a thermodynamically favoured process, the most stabilised state must be the transition state. In the case of the ester hydrolysis reaction, this is

catalysed by the presence within the active site of three amino acids that are highly conserved in hydrolytic enzymes, which together make up the catalytic triad, given by aspartate, serine and histidine. The three residues are not consecutive in the primary sequence of the protein, but are found in spatial proximity when the enzyme assumes its native three-dimensional conformation. This leads to having the three residues in the optimal distance and orientation so that, through acid-base and covalent catalysis mechanisms, they can, for example, catalyse the hydrolysis of an ester.

From a molecular point of view, hydrolysis takes place in four steps, passing through two tetrahedral intermediates and an acyl-enzyme intermediate [Fig.9].

Initially the aspartate activates histidine, which deprotonates the serine and the latter can give nucleophilic attack on the carbonyl carbon of the ester, leading to the formation of the first tetrahedral intermediate. Subsequently, the oxygen doublet descends, forming the carbonyl bond, causing the alcohol to be deprotonated by the histidine, and the acyl-enzyme intermediate is formed. Now the histidine deprotonates the water making it a better nucleophile to give attack on the carbonyl carbon, with formation of the second tetrahedral intermediate. As before, the oxygen doublet forms the C=O double bond, with the concomitant breaking of the covalent bond with serine, which is protonated by histidine. At this point the hydrolysis of the ester has been completed, and the catalytic site is ready for a new cycle of catalysis.

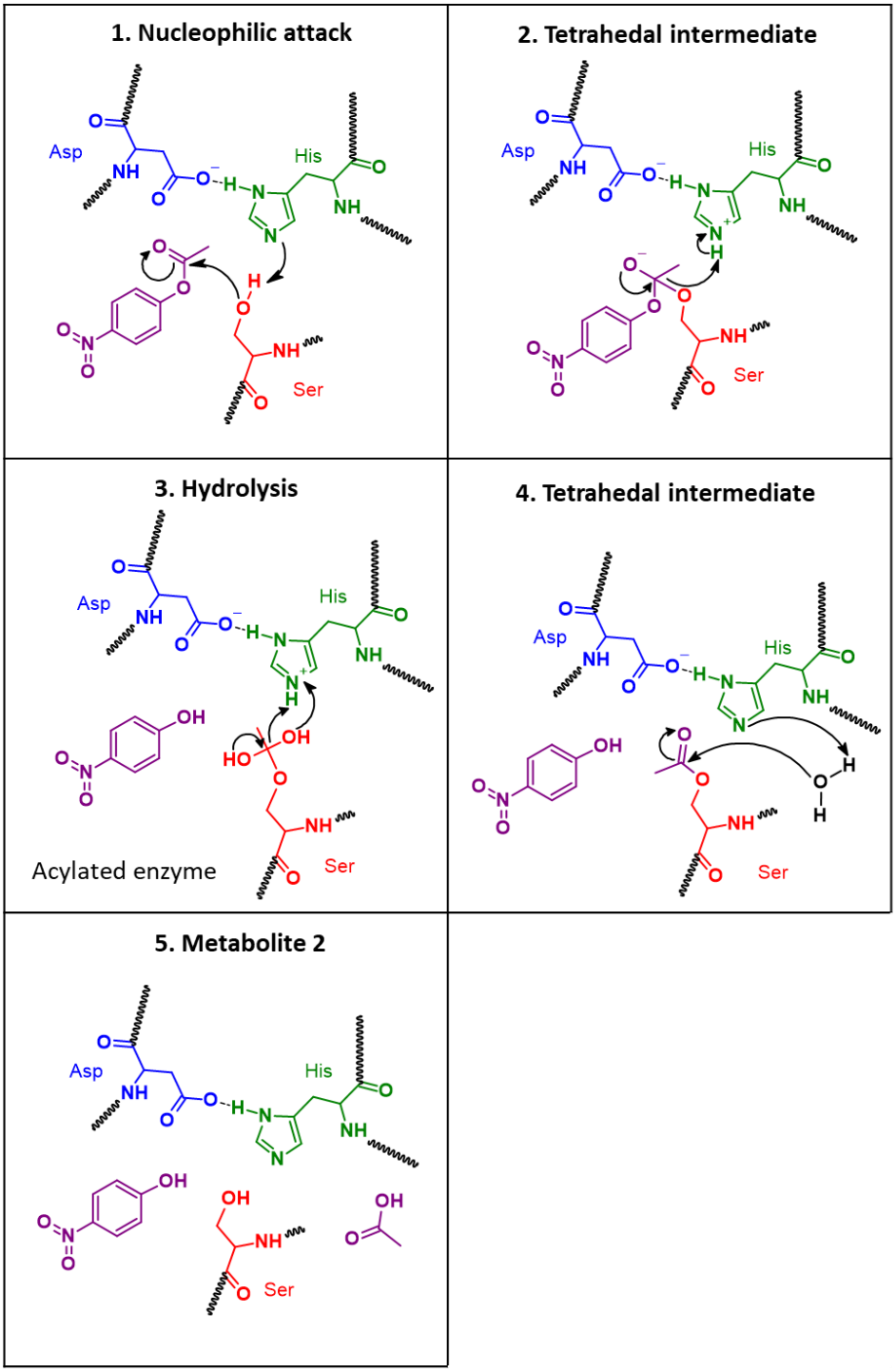

Fig.9 *Classic reaction mechanism operated by esterases.*

1.6 Peptide synthesis

Recently, small peptides have attracted attention in various scientific fields, especially in the medical, chemical and biological ones, thanks to their properties

and structural diversity, flexible conformation, ease of functionalisation, biodegradability and biocompatibility[31]. Peptides do not exceed 50-60 units, although the size limit is never clear-cut and depends on the reference context, but classic synthesis protocols result in peptides of around fifty residues, so this length can be considered as a sort of cut-off for the distinction between peptides and 'mini-proteins'[32].

The peptide bond formation reaction (coupling) involves the nucleophilic attack of the amine nitrogen of the first amino acid on the carbonyl carbon of the second residue, with the concomitant expulsion of a water molecule. Orthogonal protecting groups (e.g. fluorenylmethyloxycarbonyl chloride (Fmoc-Cl) for the amines and Fischer esterification for the carboxylic group) are required to avoid cross-reactions. For coupling to occur efficiently, activation of the carboxyl group is indispensable, which in most cases exploits carbodiimides such as EDC, DIC and DCC, which act as activators. They lead to the formation of a highly reactive compound, so it must be converted into the active ester with the aid of additives (usually HOAt, HOBt and Oxyma Pure), and only then can the coupling take place efficiently and quickly.

1.6.1 Solid phase peptide synthesis (SPPS)

Solution synthesis was the first method developed for the creation of peptides. Solution synthesis is characterised by an inexpensive and easy scale-up, the major difficulties are found in the purification steps that have to be performed at the end of each coupling, and in the impossibility of synthesising long-chain peptides, as the solubility of the macromolecule often decreases as the size increases[33].

In 1963, Merrifield synthesed a tetrapeptide for the first time using a solid-phase methodology, a technique that has become the mainstay of peptide synthesis over the years and earned Merrifield the Nobel Prize in Chemistry in 1984[34]. SPPS is a heterogeneous-phase synthesis because there is a solid support consisting of a polymer-based resin on which the peptide chain will grow through successive coupling cycles. The resin must be insoluble in all the solvents used for the synthesis, it must possess excellent and uniform loading (> 0.05 mmol/g), it must

have good swelling properties to prevent mass transport from becoming a limiting phenomenon, it must be mechanically stable and allow the filtration of reaction and solvent waste[35]. SPPS consists of coupling cycles, in which the first amino acid in the chain binds to the resin after it has been deprotected, after which the protective group must be removed from the newly added amino acid to obtain the free amino group that will form the peptide bond with the next unit, taking advantage of the latter's previously activated carboxyl group [Fig.10][36]. After each coupling and un-coupling reaction, the resin must be washed to remove excess reagents remaining in solution, which could compromise subsequent coupling cycles. At the end of peptide synthesis, a total deprotection is performed, i.e. removing all the protective groups of the chain's amino acids. Finally, it is necessary to separate the peptide chain from the resin, an operation that can be carried out concurrently with total deprotection using suitable reagents.

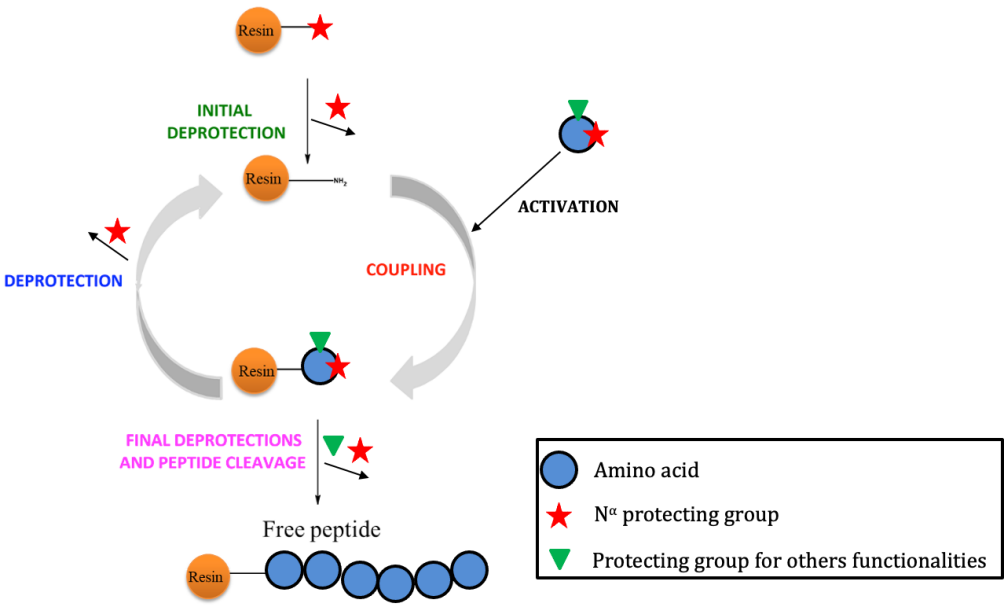

Fig.10 *General scheme of solid-phase peptide synthesis (SPPS).*

2. MATERIALS AND METHODS

2.1 Materials

2.1.1 Solvents and reagents

- Activotec: Fmoc-His(Trt)
- Alpha Aesar: $NaBH_4$
- Carbosynth: EDC*HCl
- CARLO ERBA: ACN for HPLC
- Fluka: HCl 3M in MeOH; 2,2,2-Trifluoroethanol
- GenScript: HOAt
- GL Biochem: Fmoc-Phe
- Iris Biotech GmbH: HATU; Resin Fmoc-(Rink Amide); Oxyma Pure; Fmoc-Leu; Fmoc-Ser(tBu); Fmoc-Val; Fmoc-Asp(tBu); Resin 2-chlorotrityl chloride
- Merck: GSH
- Sigma-Aldrich: pMBA; $AgNO_3$; CsOH; DMF; MeOH; Cys; NAC; NaOH; 4-chlorobenzylamine; ACN for synthesis; DIPEA; Lipoic acid; AcOEt; $NaHCO_3$; NaCl; Na_2 SO_4 ; THF; NEt_3 ; Trt-Cl; Aib; Boc_2 O; Diethylether; Petroleum ether; Hexane; Toluene; DCM; TFA; TIS; T3P 50 % w/v in AcOEt; DIC; DODT; Esterase Pseudomonas fluorescens, recombinant, from E. coli; Acetic anhydride; 2-ethyl-1-hexylamine; Sephadex lipophilic; Sephadex G-50; EtOH, $KHSO_4$.

2.1.2 Instrumentation

High-performance liquid chromatography

HPLC measurements were performed using an Agilent 1200 apparatus (Palo Alto, CA), equipped with a UV detector at various wavelengths, an Agilent extend-C18 column (5 µm, 4.6 x 250 mm) and a Phenomenex Jupiter 10u C4 300A column (250 x 4.6 mm). Eluents: A= 9:1 H_2 O/ACN, 0.05 % TFA; B= 1:9 H_2 O/ACN, 0.05 % TFA.

UV-VIS spectroscopy

UV-VIS absorption spectrum were recorded with the Agilent Cary 100 UV-VIS spectrophotometer. Quartz cuvettes with an optical path of 1 cm were used.

Circular dichroism

The instrument used for the DC analysis is Jasco J-1500. The cuvette is made of quartz, with an optical path of 0.1 cm.

Nuclear magnetic resonance

The spectrum^{1} H-NMR and H-^{11} H-TOCSY were recorded at 25 °C with the Bruker Avance400 MHz instrument. The multiplicity of the signals is indicated by: s, singlet; d, doublet; t, triplet; dd, doublet of doublets; m, multiplet.

Transmission Electron Microscopy (At the Department of Biology)

TEM images were obtained with the FEI TECAI G12 instrumentation, which uses a tungsten filament as an electron source for the thermionic effect. The liquid samples observed at TEM were prepared by placing a drop of the solution under investigation on a 400-mesh copper screen covered with a carbon film, which acts as a carrier.

2.2 Methods

2.2.1 Synthesis of $M_4Ag_{44}(pMBA)_{30}$

A solution of 154.2 mg (1.0 mmol) p-MBA in 12 mL of EtOH is prepared and placed in a flask under constant stirring at 1000 rpm. A solution consisting of 42.4 mg (0.25 mmol) of $AgNO_3$ in 21 mL of H_2 O is added to this; at this point the solution becomes turbid, indicating the formation of the insoluble precursor between silver and p-MBA. It is basified to a pH = 12 with CsOH (50% w/v) to solubilise the precursor and deprotonate the ethanol to stabilise the cluster. Now the reducing solution consisting of 94.6 mg (2.5 mmol) of $NaBH_4$ in 9 mL of H_2 O is added drop by drop. Once the reduction has started, one will notice the change in the colour of the solution from yellowish to first grey, then brown and finally, after about two hours of reaction, dark red. The nanoclusters are purified by an initial centrifugation to remove any solids formed, then precipitated with DMF to remove salts and excess pMBA. The precipitate is dissolved in a 1% (v/v) solution of acetic acid in DMF and precipitated with toluene; these procedures must be repeated several times for the precipitate to dissolve in DMF, remaining stable without the need for acidification.

2.2.1 Synthesis of AgNC_GSH and AgNC_Cys

AgNC_GSH. For the synthesis, reference is made to the experimental procedure developed by Kumar et al.[37] . Under constant stirring at 1100 rpm, 42.4 mg (0.25 mmol) of $AgNO_3$ is dissolved in a flask with 50 ml of water to which 307 mg (1 mmol) of GSH is added, leading to the formation of a whitish solution indicative of the formation of the silver thiolate precursor. The reaction is placed on ice for 30 minutes, after which the reducing solution consisting of 94.6 mg (2.5 mmol) of $NaBH_4$ in 12.5 mL of water is added dropwise. The reaction continues for about an hour until a dark red color is obtained. Purification of the nanoclusters involves an initial rotavapor concentration followed by a series of precipitation and

centrifugation steps in MeOH in order to remove salts and GSH remaining in solution. The precipitate is finally dissolved in water.

AgNC_Cys. Initially 121.2 mg (1 mmol) of Cys in 15 mL of H_2 O and place under constant stirring at 1000 rpm. The AgNO solution$_3$ (42.4 mg; 0.25 mmol in 10 mL of H_2 O) is added and the formation of the insoluble precursor is noted and allowed to equilibrate for a few minutes, after which it is basified with CsOH until a clear solution is obtained. At this point, reduction is carried out by dropwise addition of a solution of $NaBH_4$ (94.6 mg; 2.5 mmol in 8 mL of H_2 O) and allowed to react for about two hours.

2.2.2 Functionalization of $M_4Ag_{44}(pMBA)_{30}$ by the disulphide bridge method

d-pMBA synthesis. For the dimerisation of pMBA, 170 mg (5.3 mmol) of pMBA is dissolved in 10 mL of MeOH, to which 200 uL of acOH and a solution of 500 mg of I_2 dissolved in MeOH are added. A solution of 100 mg (0.9 mmol) thiosulphate in 100 mL of H_2O is added to this solution. A vacuum filtration of the resulting solution is carried out. The filtered solution is placed in the rotavapor.

Synthesis of nanoparticles The solid residue of d-pMBA obtained from the rotary evaporator is dissolved in 15 mL of EtOH and placed in a flask under stirring at 1000 rpm. To this, a solution of $AgNO_3$ (30 mg; 0.18 mmol in 10 mL of H_2 O) is added and allowed to equilibrate. The reducing solution of 77 mg (1.8 mmol) in 6 mL of H_2O is added drop by drop and allowed to react for about 3 hours. Finally, the solution is concentrated on the rotavapor, centrifuged in H_2O and the precipitate is dissolved in EtOH, resulting in a dark brown nanoparticle solution.

2.2.3 Functionalization of $M_4Ag_{44}(pMBA)_{30}$ with the pMBA tritylation method

Synthesis of the Trt-pMBA batch. 4.0 g (26 mmol) of pMBA and 7.2 g (26 mmol) of trityl chloride (Trt-Cl) are placed together in a flask and dissolved in 40 mL of DMF, with constant stirring at 1000 rpm. 9 mL (52 mmol) of DIPEA is added and allowed to react for one day. At the end of the reaction, it is rotavapor evaporated to remove the DMF and the solid residue is first dissolved in about 200 mL of AcOEt and then purified by acid, basic and brine washes (each wash is repeated 3 times). The organic phase of AcOEt contains the product, so it is anhydrified with Na_2 SO_4 to remove any remaining water and is evaporated to remove the AcOEt. The residue is dissolved with a few mL of AcOEt, precipitated with 200 mL of hexane and left overnight in the refrigerator. The solution is then vacuum filtered and the solid is recovered in 70% yield.

2.2.4 Synthesis of nanoclusters with catalytic peptide ligands

As far as the synthesis of nanoparticles using these catalytic peptides as ligands is concerned, the procedure follows that of the Desireddy group, varying volumes and concentrations accordingly.

2.2.4.1 Solid-phase synthesis of catalytic peptides

The solid-phase synthesis of peptides is based on the elongation of the amino acid sequence while it is anchored to a solid support. The main advantage of this technique is the ease with which reagents and solvents can be removed from the peptide without the need for specific steps or laborious purification techniques. The solid support consists of a resin, which is inert and insoluble with a specific functionalisation that allows the first molecule to be immobilised on the resin. Once the first amino acid is fixed on the resin via the carboxyl group, the peptide sequence

is linearly lengthened towards the N-terminus by alternating N-deprotection and amino acid coupling reactions.

The synthesis of the peptide ligands takes place in the solid phase using 2-chlorotryl resin as the support on which the peptide chain will grow. The reaction solvent is DMF and the amino acids used all have their amino groups protected with Fmoc.

Coupling of the first residue takes place in a small reactor with two outlets; one for solvent flow and one for nitrogen flow. Each step must be under nitrogen flow to ensure continuous mixing. The first amino acid can be added directly to the reactor in the presence of DIPEA and a nucleophilic substitution reaction will take place on the trityl. Synthetically, 3 grams of the 2-chlorotrityl resin is swelled using 15 mL of DMF. The bond between the resin and cysteine is achieved by preparing a solution with 3 molar equivalents of the resin loading) of the first aminoacid in 35 mL of DMF. The reaction is allowed to run for 1 hour. After washing with DMF in the reactor, the resin sites that did not react with the mix consisting of DCM/MeOH/DIPEA (80 : 15 : 5) are capped. It is stirred under nitrogen flow for 20 minutes. The resin is washed three times with DCM and then three times with DMF. At the end of the step the resin dries to obtain the solid product to be placed in the automated peptide synthesizer. Here, the Fmoc group is unblocked with piperidine 20 % v/v in DMF and the next amino acid, previously activated with DIC and Oxyma Pure, can then be added. The cycle consisting of deprotection and coupling is also repeated for the last amino acid to be introduced and for Trt-pMBA. Finally, the peptide chain is deprotected from the protecting groups and is detached from the resin with the mix consisting of TFA/DODT/H_2 O/TIS (93.5 : 1.5 : 2.5), leaving a terminal carboxyl group. The peptide is finally purified by precipitation and centrifugation with diethylether on ice [Fig.11].

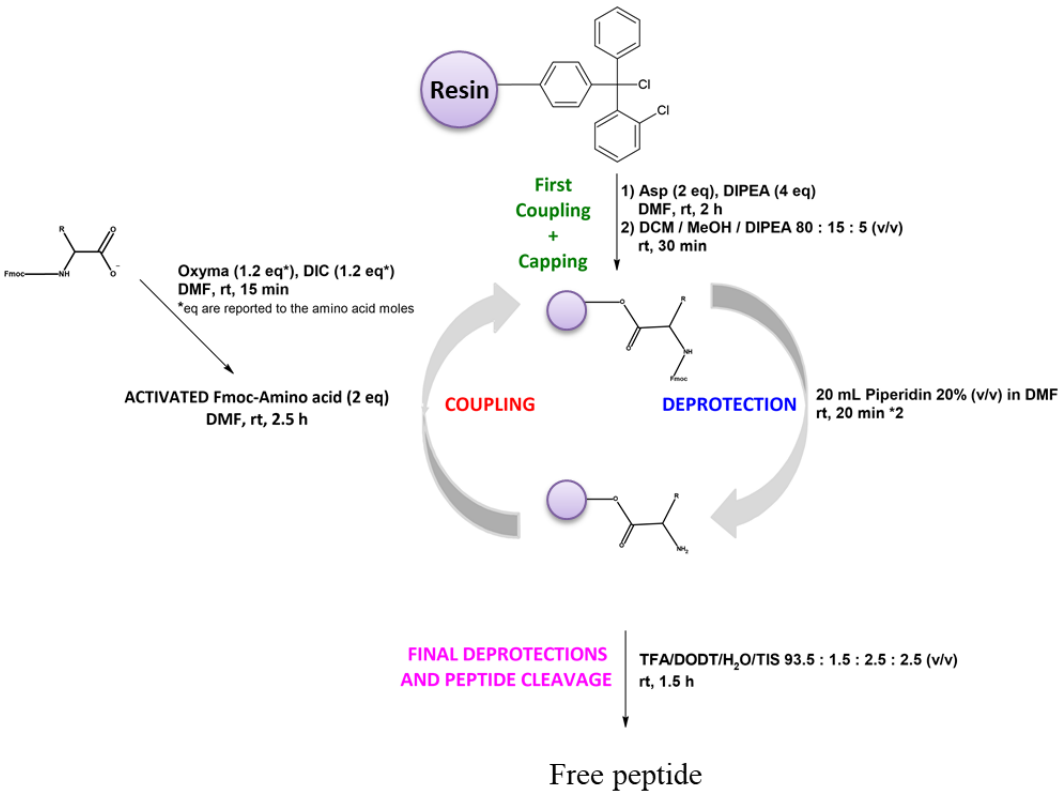

Fig.11 *General scheme of SPPS with 2-chlorotryl resin adopted in this thesis project. The amino acids are introduced in the following order: Fmoc-Asp(tBu), Fmoc-His(Trt), Fmoc-Ser(tBu). Finally, the last coupling involves Trt-pMBA.*

2.2.4.2 AgNC_P1

The P1 ligand, i.e. pMBA-Ser-His-Asp, has all three residues of the catalytic triad on the same peptide. No hydrophobic residue is added, in order to observe how the system behaves catalytically even without the creation of an apolar environment. It is assumed that the catalytic properties of this system are not due to the cooperativity of the residues on the same peptide, but most likely the synergetic effect will include amino acids on different ligands, but which are spatially close to each other on the surface of the nanocluster [Fig.12].

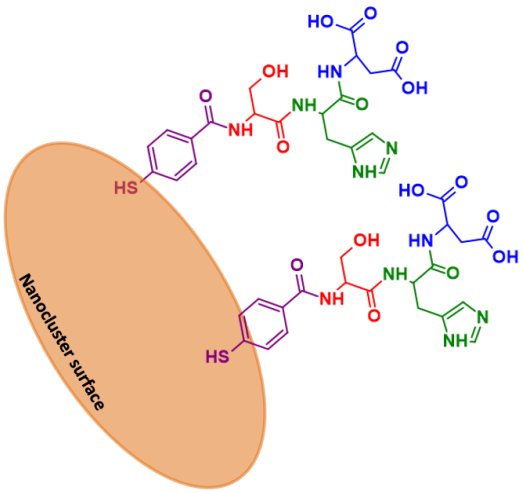

Fig.12 *Nanocluster functionalised with the P1 ligand.*

Synthesis of AgNC_P1. 183 mg (0.37 mmol) of P1 is dissolved in 12 mL of EtOH, to which a solution of $AgNO_3$ (17 mg; 0.1 mmol in 15 mL of H_2 O) is added. This is allowed to equilibrate, after which it is basified to pH = 12 with $CsOH_{(aq)}$ 50 % w/v. Dropwise reduction is carried out with a solution consisting of 38 mg (1 mmol) of $NaBH_4$ in 7 mL of H_2 O. The nanocluster formation reaction lasts for one day, after which the products are purified by gel column permeation, using Sephadex G-50 as the stationary phase.

2.2.4.3 AgNC_P1-hydrophobic-controller

In the ligand design, the next step was to maintain the three catalytic residues on the same peptide, but introducing an apolarity character to the system. This is initially introduced by adding a hydrophobic controller during the synthesis of the nanoclusters. The molecule in question is derived from the functionalisation of lipoic acid with 2-ethyl-1-hexylamine, leading to the formation of a structure that at one end has two thiols to coordinate with silver, while at the other end there is an aliphatic chain, hence apolarity [Fig.13].

Synthesis AgNC_LipoicAcid. 206.3 mg (1 mmol) of lipoic acid is dissolved in 10 mL of EtOH in a flask placed under constant stirring at 1000 rpm. The carboxylates

are basified with two equivalents of NaOH, then a 10 mL solution of H_2 O with 80 mg NaOH is prepared. Silver nitrate solution (42.4 mg; 0.25 mmol in 21 mL of H_2O) is added and the solution is cooled on ice for 15 min. It is reduced with a solution of $NaBH_4$ (94.6 mg; 2.5 mmol in 8 mL of H_2 O) drop by drop and the reaction is kept on ice for 30 min, after which it is allowed to continue at room temperature for a day. Eventually, a red nanoparticle solution is obtained, which is precipitated in ACN to remove unreacted compounds. The precipitate is finally dissolved in H_2O.

Synthesis of the hydrophobic controller Lipoate(2-ethyl-1-hexylamine). 400 mg (1.9 mmol) lipoic acid is dissolved in 15 mL ACN and activated with 259 mg (1.9 mmol) HOAt, 435 mg (2.3 mmol) EDC*HCl for 10 min. Afterwards, 0.8 mL (4.9 mmol) of 2-ethyl-1-hexylamine and 0.5 mL (3.6 mmol) of NEt_3 are added and the coupling is continued for one day. Solid suspensions are formed during the reaction, which are partly removed by adding a few mL of DCM. The product is purified by an initial evaporation of the solvent in rotavapor, followed by dissolution of the solid residue in 50 mL of AcOEt. Acid washing with $KHSO_4$, basic washing with $NaHCO_3$ and brine washing. The organic phase containing the product is evaporated, the residue is dissolved in DCM and allowed to dry in a vial to obtain the solid Lipoate(2-ethyl-1-hexylamine).

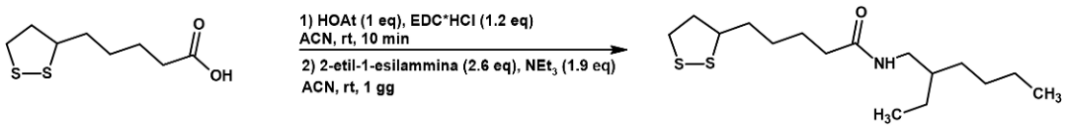

Fig.13 *Schematic of the coupling reaction between lipoic acid and 2-ethyl-1-hexylamine.*

Synthesis of pMBA-hydrophobic-controller. The nanoparticles are synthesised by initially mixing the catalytic ligand P1 with the hydrophobic controller Lipoate(2-ethyl-1-hexylamine). Different molar ratios between the two molecules are tested, and it is found that as the percentage of apolar ligand increases, the system becomes increasingly insoluble. As a result, the optimal ratio identified has 30 % in moles of hydrophobic controller compared to P1 [Fig.14].

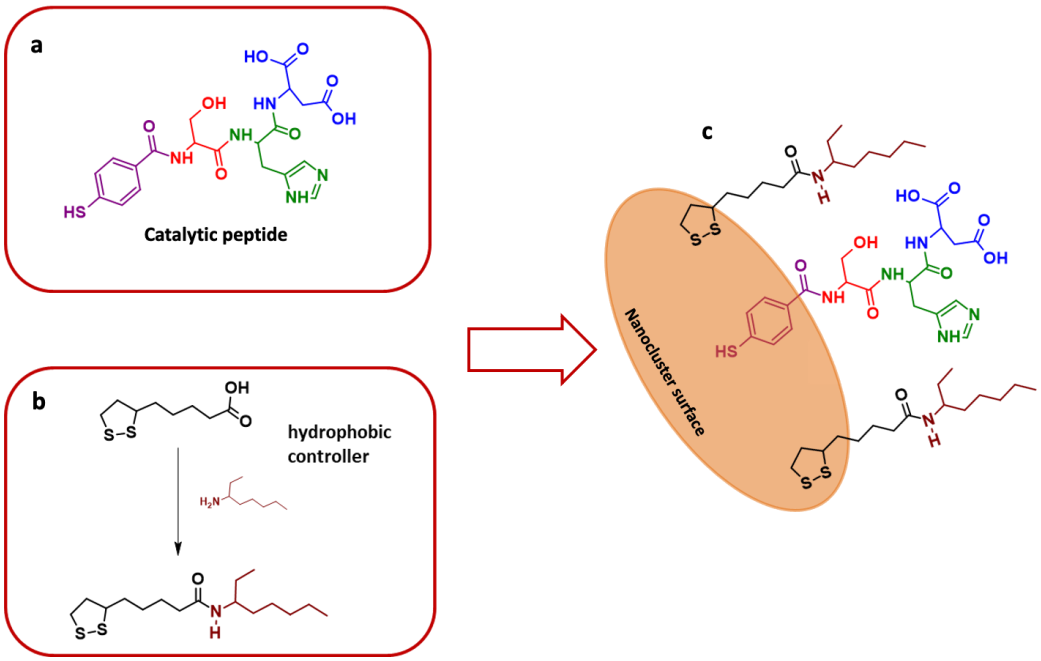

[Fig.14] Molecular structure of the catalytic peptide ligand P1 (a), the hydrophobic controller Lipoate(2-ethyl-1-hexylamine) (b) and the hypothetical surface of the nanocluster when its synthesis takes place in the presence of the two preceding molecules (c).

Synthesis of AgNC_P1-30%mol. A solution is prepared in 15 mL of EtOH with 183 mg (0.37 mmol) of pMBA-SHD and 35 mg (0.11 mmol) of Lipoate(2-ethyl-1-hexylamine). Another solution consisting of 20 mg (0.12 mmol) of $AgNO_3$ in 10 mL of H_2 O is added to this solution. It is allowed to equilibrate, after which it is basified to pH = 12 with $CsOH_{(aq)}$ 50 % w/v. Dropwise reduction is carried out with a solution consisting of 45 mg (1.2 mmol) of $NaBH_4$ in 7 mL of H_2 O. The nanocluster formation reaction lasts for one day, after which the products are purified by column permeation gel, using Sephadex G-50 as the stationary phase.

2.2.4.4 Helices ligands

As mentioned several times in the past paragraphs, in order to obtain a system capable of mimicking the catalytic properties of the active site of esterases, it is necessary to have the catalytic residues in a precise spatial arrangement, and in a hydrophobic environment. Apolarity of the active site is necessary so that the pKa of the catalytic residues can be such as to permit acid and basic catalysis, i.e. the fundamental steps in the enzymatic hydrolysis of an esterase.

In order to recreate a three-dimensional reciprocal arrangement of the three catalytic residues, two helical peptide ligands were synthesised, namely a His-helix containing the histidine of the catalytic triad in its peptide sequence and an Asp/Ser-helix containing aspartate and serine. The hope is that by binding the two helices to the nanoparticle, these helices can be close together and assume a conformation such that a wild-type esterase-like pocket can be recreated in its three-dimensionality [Fig.15] That is, we expect a three-dimensional peptide structure that can facilitate the fattening of the substrate in the pocket of the active site and the encounter between the substrate and the residues of the catalytic triad, thus facilitating the catalysis of the reaction in a protected peptide environment.

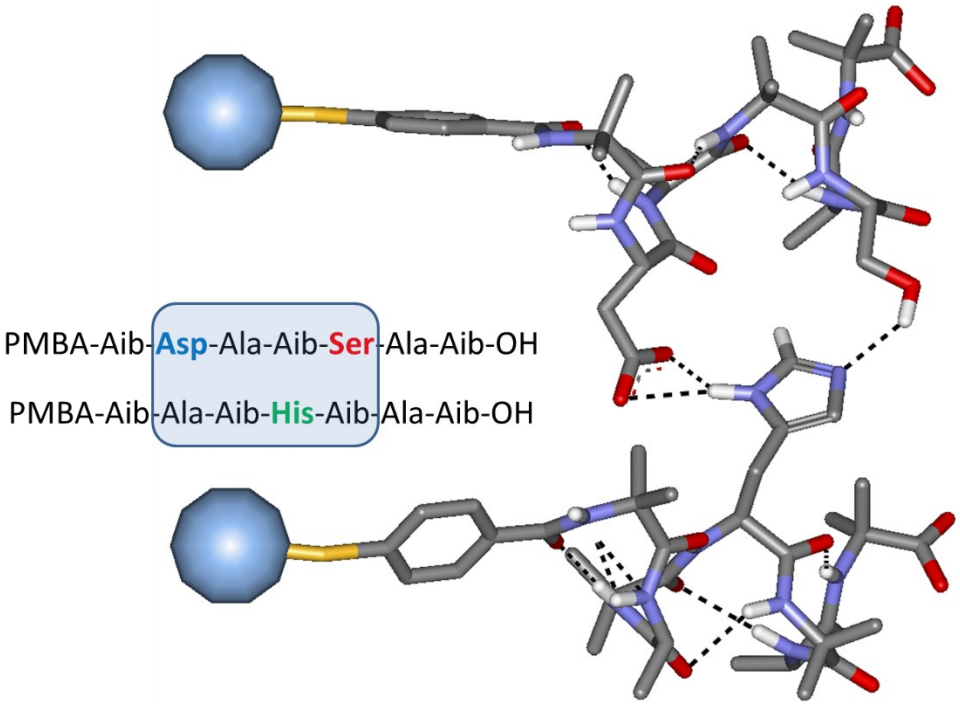

Fig.15 *The two helices on the surface of the nanocluster recreate a three-dimensional conformation of the catalytic triad.*

3. RESULTS AND DISCUSSION

3.1 Synthesis of $M_4Ag_{44}(pMBA)_{30}$

The aim of this project is to synthesise nanoclusters formed from the combination of metallic silver atoms and small peptides, which together lead to the formation of structures with catalytic properties towards the hydrolysis of the ester bond. The aim is to obtain well-defined unimolecular structures, characterised by a reduced degree of polydispersion, in order to know and control exactly the composition of the nanosystem to be exploited.

To this end, it was decided to base our studies on silver nanoclusters synthesised according to the procedure devised by Desireddy's group[33] , given their excellent stability and easy synthesis procedure. The aim is to exploit the precise spatial arrangement of the silver atoms and pMBA molecules within the final nanocluster structure, but with the intention of being able to recreate the same well-defined situation by using ligands consisting of pMBA functionalised with small peptides.

In the first step of this study, the synthesis of 'ultra-stable' silver nanoclusters was replicated following Desireddy's approach, in which silver nitrate and pMBA are initially dissolved in a solvent consisting of the water/ethanol mixture, in which the complexation of the two molecular players will take place. Subsequent basification and reduction will lead to the formation of dark red coloured nanoclusters. These were analysed by UV-VIS absorption to compare their spectrum [Fig.16(B)] with that obtained by Desireddy's group [Fig.16(A)], which is taken as a reference for our analysis.

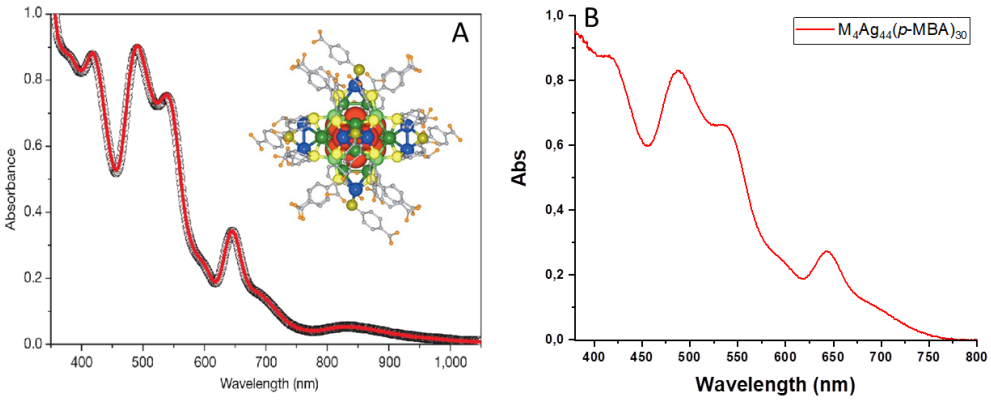

Fig.16 *Comparison of UV-VIS absorption spectrum of nanoclusters* $M_4\ Ag_{44}\ (pMBA)_{30}$ *obtained by Desireddy's group (A) and in our laboratory (B).*

Both spectrum show essentially four defined peaks and not a plasmonic band that often characterises nanoparticle syntheses, an indication that nanoclusters composed of silver and pMBA make up a system with molecular electronic confinement characteristics, such that they can be described by the formula $Ag_{44}\ (pMBA)_{30}$.

The spectrum we obtained shows the same four well-defined peaks (at around 415 nm; 490 nm; 540 nm; 645 nm) and less well-defined peaks (595 nm; 695 nm), indicative of the correct synthesis of the molecular structure sought. Unfortunately, it was also not possible to identify the absorption band at around 850 nm due to the limitations of our spectrophotometer.

Such an absorption spectrum is characteristic of small clusters composed of a few silver atoms, which are characterised by molecular-like optical transitions, exhibiting one or more absorption maxima. This is valid as long as the cluster size is small, since as the size increases, the nanosystem begins to develop a plasmonic absorption band[(38)] .

3.2 AgNC_GSH and AgNC_Cys

It is desired to investigate whether other small molecules such as glutathione and cysteine are able, by exploiting the interaction between their sulfide group and silver, to form nanoclusters of precise composition as in the case of pMBA. This

would expand the range of substrates that can be used in the synthesis of silver nanoclusters, perhaps discovering nanostructures with new three-dimensional organizations and properties.

The attempted synthesis of these nanoclusters follows, in the case of glutathione, the synthesis methodology employed by Kumar's group[37] , while in the case of cysteine, the procedure of Desireddy's group is followed by changing the organic molecule that is complexed to silver and appropriately varying the reaction conditions. In order to verify whether the syntheses resulted in the formation of small nanoclusters or simple plasmonic nanoparticles, the products are analyzed according to their UV-VIS absorption spectrum [Fig.17].

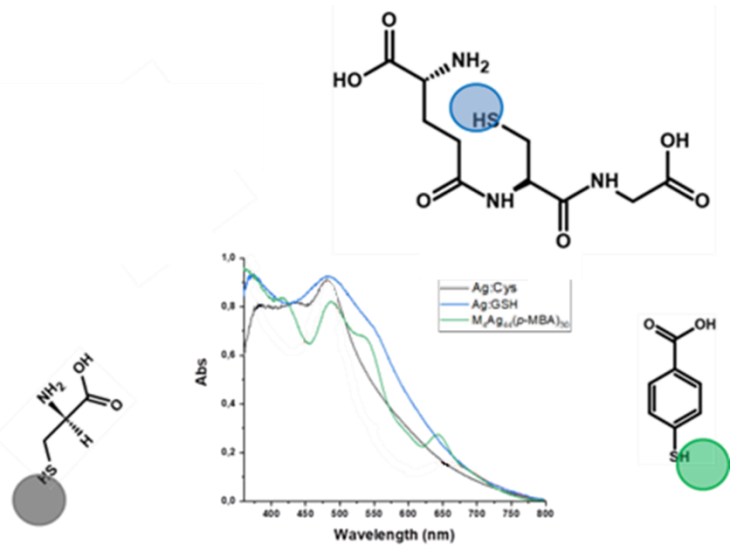

Fig.17 *Comparison of absorption spectrum of AgNC_GSH, AgNC_Cys and* M_4 *Ag nanoclusters*$_{44}$ *(pMBA)*$_{30}$ *.*

None of the synthesized nanoparticles present an absorption spectrum perfectly overlapping with that of Ag nanoclusters$_{44}$ (pMBA)$_{30}$. Ag:Cys presents a peak at 480 nm, a slight hump at 605 nm and another less defined band at 435 nm. In the 450-600 nm range, the pattern of Ag:GSH resembles that of Ag nanoclusters$_{44}$ (pMBA)$_{30}$ with the two peaks much less pronounced and the absence of the peak at 650 nm.

Although the spectrum are different from each other, it is not necessarily the case that these refer to different structures of the silver metal core, since the different

nature of the binder forming the shell of the nanoclusters/nanoparticles could also influence the position, width and height of the absorption peaks[37] .
Despite these differences, the experiment provided insight into how even by changing the nature of the binder, nanoparticles are able to form due to the interaction between silver and thiol.

3.3 Functionalisation of the pMBA

The presence of amine groups is a problem from the point of view of the synthesis of nanoclusters, since the nitrogen atoms could also coordinate with silver as an alternative to thiol, forming different and heterogeneous structures. Moreover, a hypothetical functionalisation of these molecules would be complicated by the presence of multiple functional groups.

pMBA only has a thiol, which will be used to coordinate with silver, and a carboxylic function, which can be functionalised by trying to synthesise pMBA derivatives for use as ligands in the synthesis of nanoclusters. The idea is to obtain a nanocluster with a metal core identical to that of M_4 Ag_{44} $(pMBA)_{30}$, in which only the type and obviously the spatial arrangement of the molecules that make up the shell of this system vary.

In this regard, there are two options: 1) Functionalise the pMBA after synthesising the $M_4Ag_{44}(pMBA)_{30}$ by exploiting the external carboxyl groups; 2) Synthesise the ligand of interest and use it together with silver nitrate in the synthesis of nanoclusters. Both approaches were tested, but the focus was more on the second.

3.3.1 Pre-synthesis functionalization

In this approach, the aim is to synthesise the ligand consisting of pMBA functionalised with a small peptide, using solution and solid-phase peptide

synthesis techniques, and then to exploit the final molecule in the Desireddy group procedure to obtain the nanoclusters of interest. The hope is to exploit the interaction between pMBA and silver to form the same reference nanoclusters, i.e. with the same spatial arrangement of the atoms forming the metal core, but carrying a peptide chain on the outside.

It is evident that in these circumstances, the formation of the same three-dimensional structure is made difficult by having a larger ligand, thus characterised by a greater steric size, which could alter the number and arrangement of the molecules that make up the system's shell.

For this process of functionalising pMBA pre-synthesis to be successful, the reactivity of this molecule must be taken into account. Its derivatisation is in fact complicated by the presence of the thiol group, also a reactive centre, but which must remain unaltered in order for it to coordinate with the silver atoms.

The first strategy consists of a pre-dimerisation of pMBA by forming a disulphide bridge between two pMBA molecules, leaving free two external carboxyl functionalities that can be functionalised by coupling with an amine. The disulphide bridge will then be reduced during nanoparticle synthesis by $NaBH_4$.

The second method involves the tritiation of the sulphide group of pMBA, which is then removed by acid treatment after all the functionalisations necessary for the synthesis of the ligand have been carried out. This is the method that has been focused on the most.

3.3.2 Functionalisation by disulphide bridge method

The first method of protecting the sulphide group of pMBA involves dimerising this molecule, thus forming a disulphide dimer by means of a disulphide bridge, and leaving the carboxyl ends free to be functionalised. Once the ligand of interest has been synthesised, it will be used in its oxidised form in nanoparticle synthesis, since the reduction of the disulphide bridge will take place in the NaBH addition step [Fig.18].

Once it had been proven that the presence of a disulphide bridge on the ligand does not adversely affect the synthesis of nanoparticles/nanoclusters, the next step was

to dimerise the pMBA and then functionalise it, without the risk of unwanted cross-reactions of thiol groups. In the reduction step, the disulphide bridge is reduced and thus each ligand molecule has a single thiol group that can cross-react with silver.

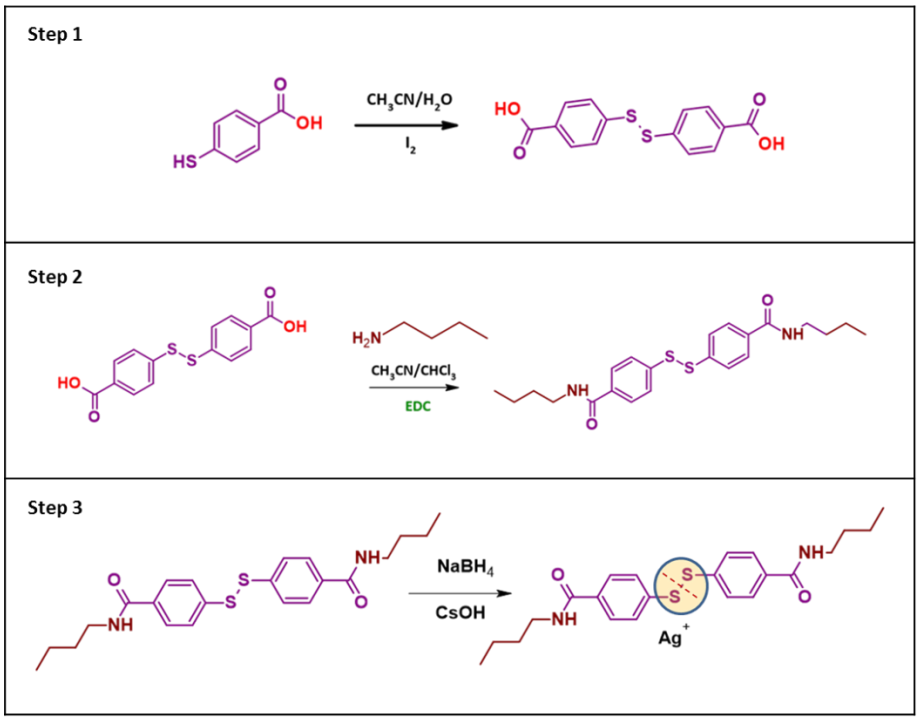

Fig.18 *Reaction diagram of pMBA dimerisation.*

The resulting molecule was used as a ligand in the synthesis of nanoparticles, leading to the formation of systems characterised by a plasmonic absorption spectrum [Fig.19].

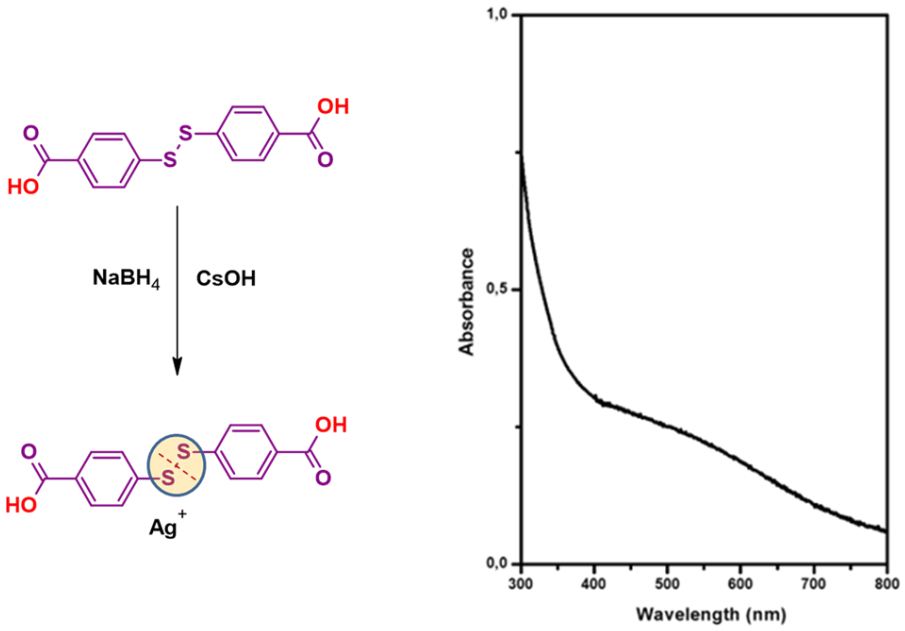

Fig.19 *UV spectrum of nanoparticles functionalized by disulphide bridge method. The absorption spectrum of the new nanoparticles exhibits a plasmonic band centred at around 550 nm. Plasmonic absorption can occur both when the nanoparticle size is large and when aggregation phenomena are present.*

3.4 Synthesis of AgNC_LipoicAcid

The idea of wanting to exploit a ligand with a disulphide bridge in the synthesis of nanoparticles does not take into account the influence this could have on the reaction. The hypothesis is to have the concomitant reduction of the disulphide bridge and silver, with the subsequent formation of a three-dimensional structure given by the combination of the metal atoms and the thiol. To verify this, it was decided to test the synthesis of nanoparticles using lipoic acid as a ligand, given the presence of an internal disulphide bridge on this molecule.

From an experimental point of view, the operational steps are the same as the procedure devised by Desireddy's group.

Eventually, a bright red solution of nanoparticles is obtained, which is purified by precipitation in ACN. The precipitate is finally dissolved in H_2 O and characterised in a spectrophotometer. Already from a visual point of view, it can therefore be

assumed that the lipoic acid nanoparticles have a different three-dimensional structure to that of the nanoclusters $M_4Ag_{44}(pMBA)_{30}$.

The basification step with NaOH serves to have the deprotonated carboxylic functions on the outside of the nanoparticles, hoping for their stabilisation by means of an electrostatic repulsive force operated by the negative charges, as is often exploited by common syntheses of gold nanoparticles stabilised with citrate[39]. Basification allowed the formation of nanoparticles that retained their red colouring for many hours, especially by storing the nanoparticle solution in a refrigerator at 4°C, which causes the suspension to remain bright red even weeks after synthesis.

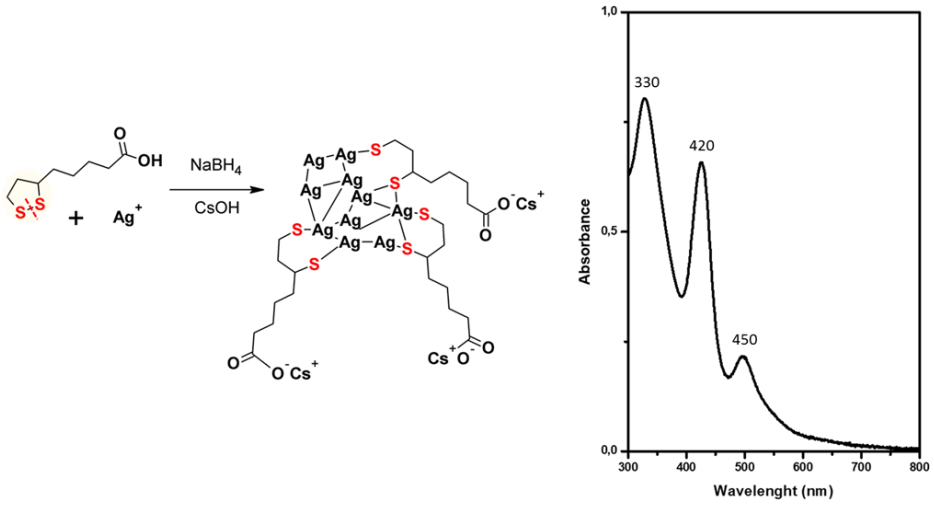

Fig.20 *UV sprectra of AgNC_LipoicAcid*

The spectrum [Fig.20] has three bands at 330 nm, 420 nm and 450 nm. Compared to the spectrum of AgNC_pMBA, the bands from 500 to 800 nm are not present. It was certainly to be expected that the spectrum would not be totally superimposable with that of the nanoclusters M_4 Ag_{44} $(pMBA)_{30}$, since lipoic acid, once reduced, has two sulphide groups, which can coordinate differently with the silver atoms than with pMBA, which has only one sulphide. The geometry of the structure, and thus the relative arrangement of the silver atoms and the ligand molecules, particularly influences the final shape of the nanoparticle and its size, leading to certain electronic transitions, which are reflected in an absorption spectrum of various kinds. Despite this, the spectrum of Ag:Lipoic nanoparticles do not present a single broad plasmonic band, but are characterised by two well-defined bands, a situation often encountered when dealing with nanoclusters.

The small size of the nanoclusters consisting of lipoic acid is confirmed by TEM images, where it can be seen that the diameter of the nanosystems is around 5 nm [Fig.21].

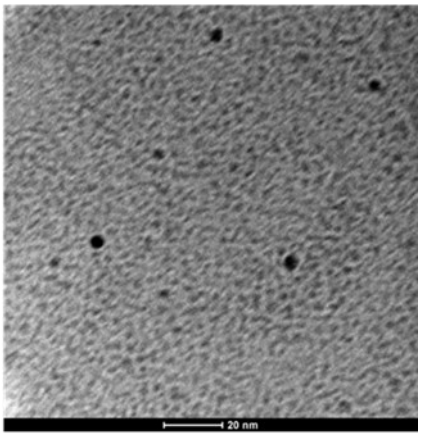

Fig.21 *TEM image of AgNC_LipoicAcid.*

The hypothesis is that ligands consisting of lipoic acid and derivatives are capable of forming nanoclusters of small size and precise geometry, due to the way in which silver atoms combine with free sulphides. This way of combining will certainly differ from that of pMBA, since in the case of lipoic acid, it will be the case that the same ligand molecule can coordinate to several silver atoms, given the presence of the two sulphides.

3.5 Trt-pMBA batch

Trityl is one of the most common protecting groups used in organic syntheses, due to its stability under neutral and basic conditions, a characteristic that allows it to be orthogonal to the other protecting groups often used in peptide syntheses (e.g. Acm and tBu). Usually trityl is exploited for the protection of alcohol groups, e.g. of carbohydrates[(40)] , but it is also used for the protection of thiol groups, e.g. of cysteines in SPPS processes[(41)] .

In the present project, the tritiation of pMBA is exploited to obtain a molecule that has carboxylic acid as its only reactive centre, which can then be activated and used

in coupling reactions with free amines to form ligands for the synthesis of nanoparticles.

From an experimental point of view, mercaptobenzoic acid reacts with trityl chloride in a basic environment in DMF, with the subsequent formation of Trt-pMBA [Fig.22]. Once the complete ligand is synthesised, it is necessary to remove the trityl in order to make the thiol available for interaction with silver atoms during nanoparticle synthesis. The removal involves acid treatment with TFA in the presence of scavengers, i.e. molecules such as TIS, which serve to capture the carbocation formed during deprotection, preventing them from reacting with the nucleophilic groups present in the final ligand.

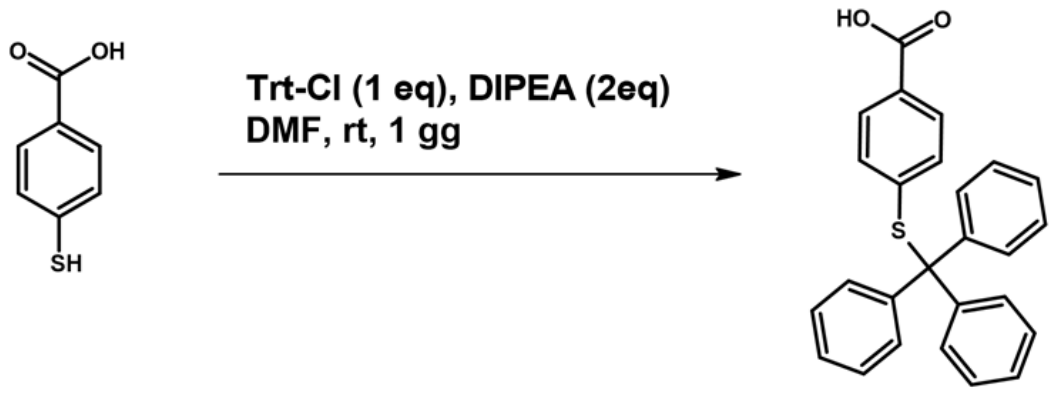

Fig.22 *Reaction diagram of pMBA tritiation.*

The nature of the ligand is what we can control so that nanoparticles/nanoclusters with precise properties are formed.

3.6 Catalytic peptide ligands

Once it was ascertained that the formation of nanoparticles also took place with ligands consisting of pMBA derivatives, the focus was on the synthesis of peptides that could perform a catalytic function. The aim is to create a favourable environment on the NC surface for the ester hydrolysis reaction, mimicking the structural organisation that characterises the enzyme catalytic pocket. It is necessary that the catalytic residues (aspartate, serine and histidine) are present, and that they

have a precise spatial arrangement such that catalysis can take place. Also important is the hydrophobic character of the system, which must allow stabilisation of the substrate to be hydrolysed and raise the pKa of the catalytic residues in order to have the correct acid and basic catalysis properties.

Through solid-phase peptide synthesis, the next ligand molecules were then synthesised: pMBA-P1 and pMBA-helices.

3.6.1 Ligand P1

The second hypothesised ligand, P1, has all three residues of the catalytic triad on the same peptide. It is observed how the system behaves catalytically. It is hypothesised that the catalytic properties of this system are not due to the cooperativity of the residues on the same peptide, but most probably the synergetic effect will include the amino acids on different ligands, but which are spatially close to each other on the surface of the nanocluster [Fig.23].

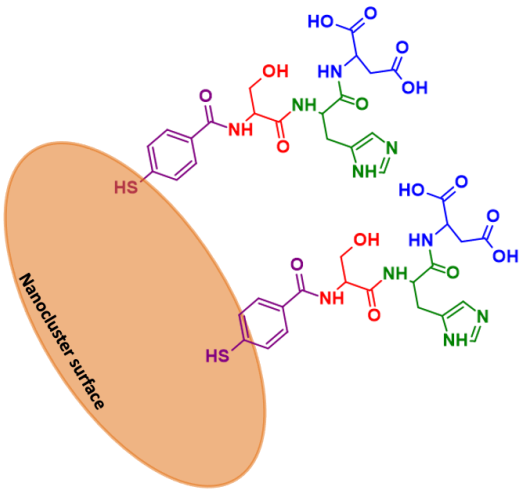

Fig.23 *Representation of the hypothetical nanocluster surface when its synthesis takes place in the presence of the pMBA-SHD ligand.*

3.6.2 AgNC_P1

Similar to what has been seen previously, the new P1 ligand is used in the synthesis of nanoclusters, following the procedure of the Desireddy group, suitably modified. The purification involves an SEC (size-exclusion chromatography) column.

3.7 AgNC_hydrophobic-controller

It shows a red colouration and a UV-VIS absorption spectrum highly overlapping with that of AgNC_LipoicAcid [Fig.24].

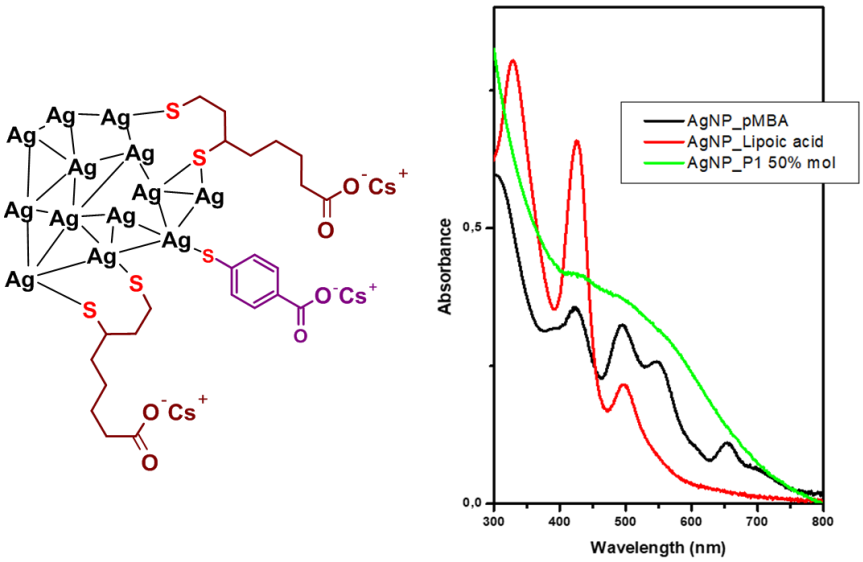

Fig.24 *Comparison of absorption spectrum.*

Once AgNC_LipoicAcid had been synthesised, the question arose as to whether a similar result could be achieved by modifying the ligand structure, e.g. by forming a peptide bond by exploiting the carboxyl functionality of lipoic acid and the amine group of 2-ethyl-1-hexalamine. In short, the lipoic acid is activated in ACN with EDC*HCl/HOAt, after which the newly formed active ester can undergo the coupling reaction with 2-ethyl-1-hexalamine [Fig.25].

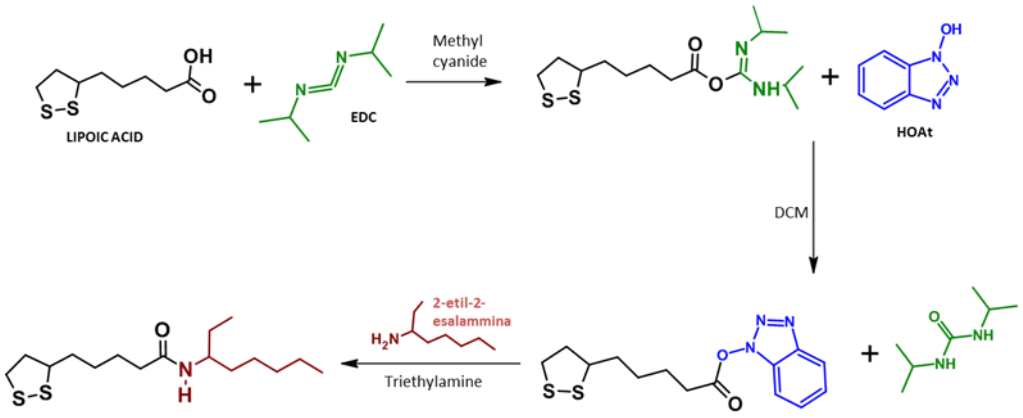

Fig.25 *Schematic of the coupling reaction between lipoic acid and 2-ethyl-1-hexylamine.*

In order to obtain a system capable of mimicking the catalytic properties of the active site of esterases, it is necessary to have the catalytic residues in a precise spatial arrangement, and in a hydrophobic environment. The apolarity of the active site is necessary so that the pKa of the catalytic residues can be such that the acid and basic catalysis, i.e. the fundamental steps in the enzymatic hydrolysis of an esterase, can take place.

This new ligand was then exploited for the formation of nanoparticles (using the same synthesis protocol), which show the same red colouration and a UV-VIS absorption spectrum highly superimposable to that of Agnc_LipoicAcid [Fig.19].

In the ligand design, the next step was to maintain the three catalytic residues on the same peptide, but introducing an apolarity character to the system. This is initially introduced by adding a hydrophobic controller during the synthesis of the nanoclusters. The molecule in question is derived from the functionalisation of lipoic acid with 2-ethyl-1-hexylamine, leading to the formation of a structure that at one end has two thiols to coordinate with silver, while at the other end there is an aliphatic chain, hence apolarity.

3.7.1 AgNC_P1-30%mol

The synthesis of these nanoclusters involves the initial preparation of an alcohol solution of the P1 ligand and hydrophobic controller. The next steps are the addition

of silver nitrate, basification with CsOH and reduction with sodium borohydride. At the end of the synthesis, the nanoclusters are purified by gel column permeation.

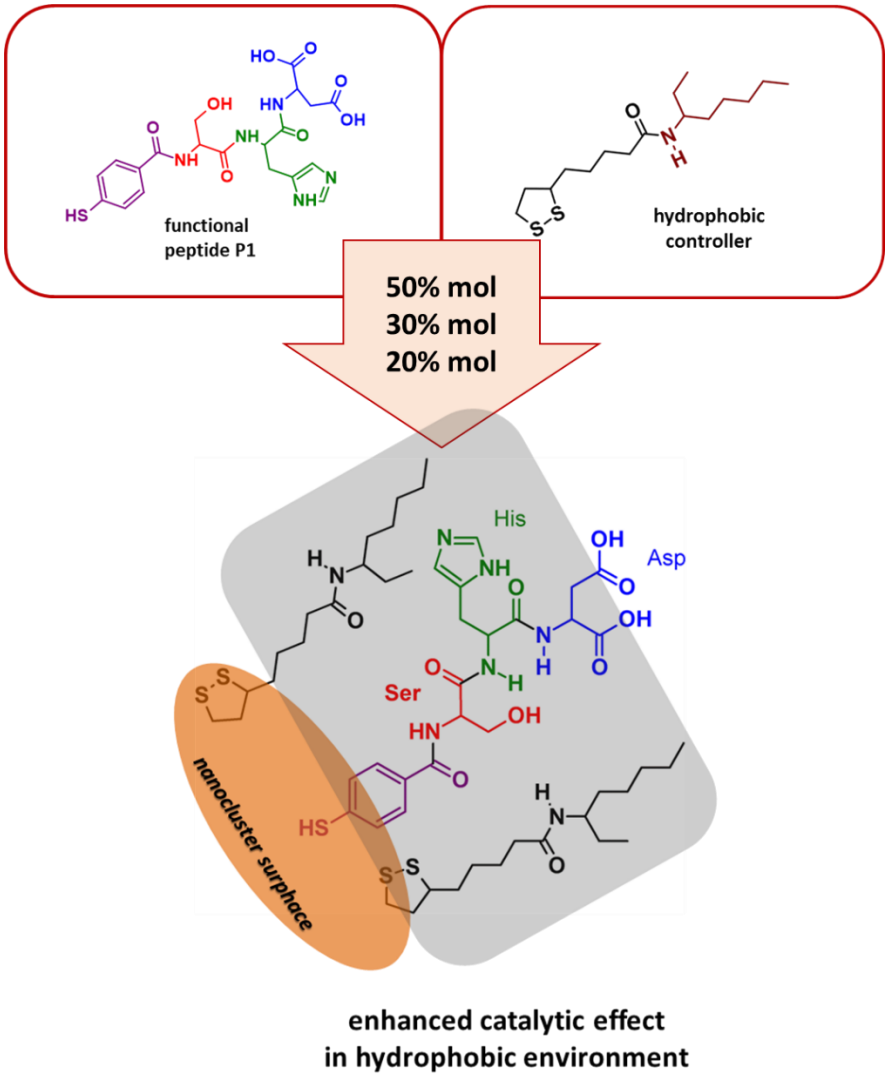

Fig.26 *Molecular structure of the catalytic peptide ligand pMBA-SHD (a), of the hydrophobic controller Lipoate(2-ethyl-1-hexylamine) (b) and of the hypothetical nanocluster surface when its synthesis takes place in the presence of the two preceding molecules (c).*

Different molar ratios between the two molecules are tested, and it is found that as the percentage of apolar ligand increases, the system becomes increasingly insoluble. The optimal ratio found has 30 per cent in moles of hydrophobic controller compared to P1 [Fig.26].

3.8 Helix ligands

His-helix. Fig.27 shows the structure of the His-helix ligand. The peptide ligand contains 7 residues with an alternating alanine and Aib in order to obtain a helical conformation and a histidine in a central position to recreate one of the three residues of the catalytic triad.

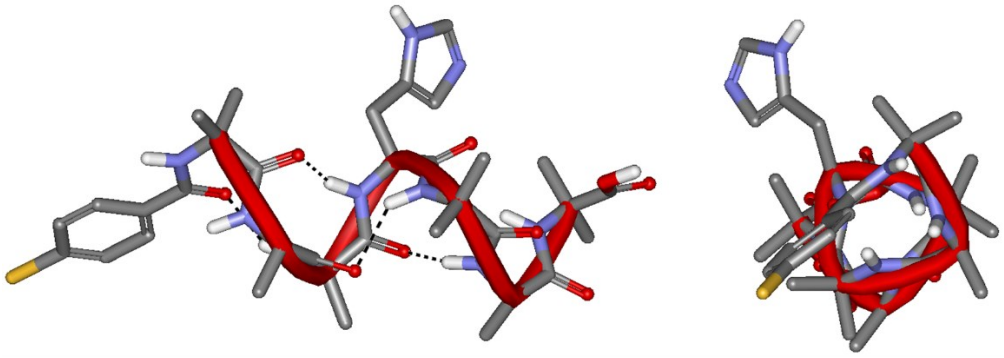

pMBA-Aib-Ala-Aib-**His-**Aib-Ala-Aib-OH

Fig.27 *Primary and secondary structure of the His-helix ligand.*

Nanoclusters containing only this ligand are synthesised to be used as a control for kinetic measurements. At the end of the chapter, the results of characterisation analyses of the synthesised peptide are reported, confirming the primary and secondary structure drawn.

Asp/Ser-helix ligand. Fig.28 shows the structure assumed by the Asp/Ser-helix ligand. The peptide ligand contains 7 residues with an alternation of alanine and Aib in order to obtain a helical conformation and also has an aspartate and a serine in order to give a three-dimensional conformation of the catalytic triad.

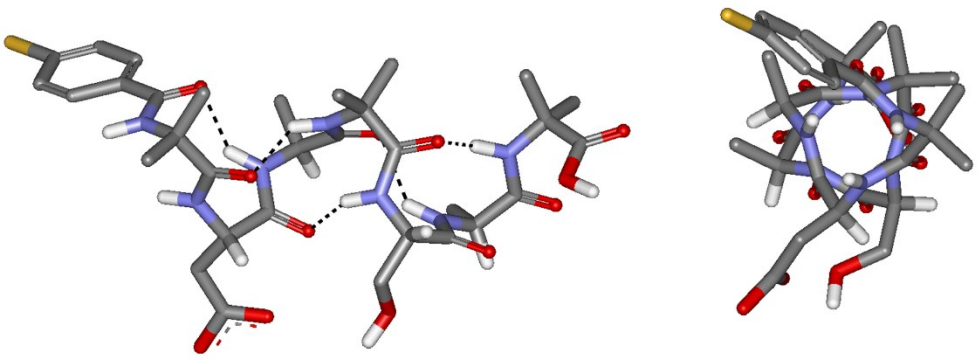

PMBA-Aib-Asp-Ala-Aib-Ser-Ala-Aib-OH

Fig.28 *Primary and secondary structure of the His-helix ligand.*

Nanoclusters containing only this ligand are synthesised to be used as a control for kinetic measurements. At the end of the chapter, the results of characterisation analyses of the synthesised peptide are reported, confirming the primary and secondary structure drawn.

3.8 Kinetic analysis

The aim of this thesis project is to be able to synthesise nanosystems, in particular nanoclusters, with catalytic properties against ester bond hydrolysis. The nanoclusters arise from the combination of metallic silver and peptide ligands. The design of the ligand has been studied in detail, so that a kind of hydrophobic site is created on the surface of the nanocluster, attempting to mimic the organisation of the enzyme catalytic pocket. The achievement of a stable and optimised conformation of the nanocluster's catalytic site should lead to the acquisition of a more or less high catalytic efficiency, depending on the reciprocal spatial arrangement of the residues and the hydrophobic environment created on the system. The catalytic properties of the nanoclusters synthesised with the different ligand molecules are then analysed on the hydrolysis reaction of 4-nitrophenylacetate (pNPA) [Fig.29]. The reaction produces the 4-nitrophenate ion, the formation of which can be easily followed by measuring the absorbance at 400 nm, i.e. the wavelength at which the absorption maximum occurs. Experimentally,

the catalysts are dissolved in a PBS buffer at pH 7.8, to which the substrate to be hydrolysed is then added. As soon as the 4-nitrophenylacetate is introduced, the absorbance is measured at 400 nm, repeating the measurement at different times in a constant manner as the reaction proceeds. If the system were truly capable of catalysing the reaction, there should be an increase in absorbance at 400 nm over time, clearly distinguishable from the simple degradation of the substrate in the test buffer.

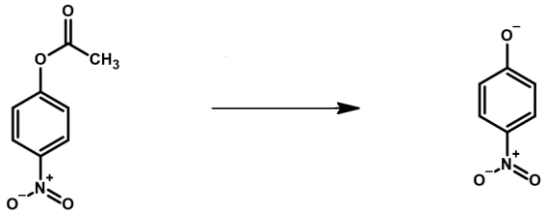

Fig.29 *Reaction diagram of the hydrolysis of 4-nitrophenylacetate.*

3.8.1 Reference kinetics - Enzyme catalysis

In this project, we aspire to synthesise catalytic systems in the image and likeness of enzymes, i.e. biological macromolecules that evolution has selected specifically for their ability to catalyse certain chemical reactions. In order to attribute a meaningful value to the catalytic properties of the nanoclusters to be analysed, it is necessary to have a reference, i.e. a kinetic model based on the performance of an enzyme. The esterase of recombinant Pseudomonas fluorescens in Escherichia coli is our reference and its catalytic efficiency was analysed on the hydrolysis reaction of pNPA [Fig.30(A)].

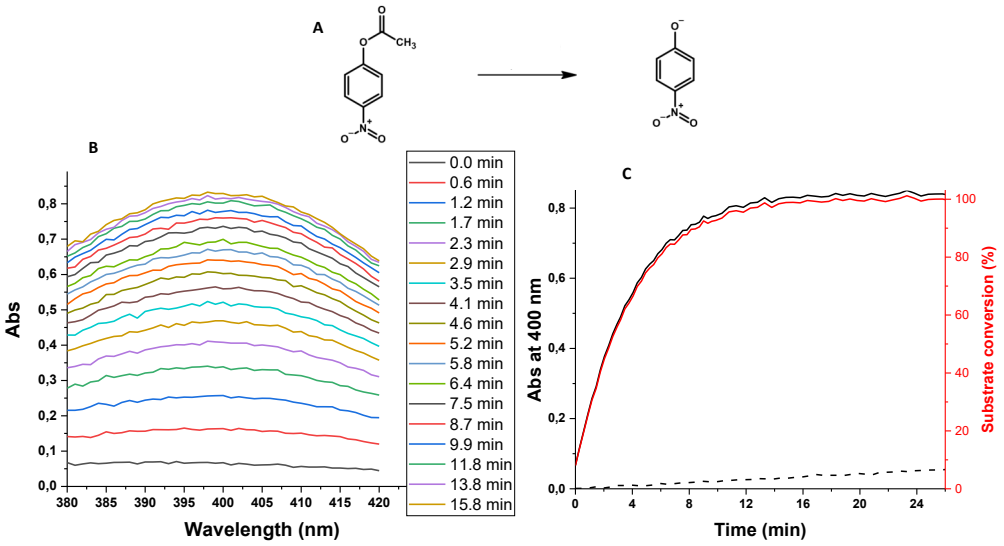

Fig.30 *Hydrolysis reaction to be catalysed (A), evolution of the absorbance spectrum of the esterase-catalysed reaction over time, measured between 380 and 420 nm (B), evolution of the absorbance at 400 nm (in black, esterase-catalysed reaction), substrate conversion (in red, esterase-catalysed reaction) and absorbance at 400 nm (in dashed black, non-catalysed reaction) over time (C).*

The graph [Fig.30(B)] shows how the absorption spectrum of the reaction varies between 380 and 420 nm, when it is catalysed by esterase. It can be seen that in the first 8 minutes the absorbance increases very quickly, while towards the end of the experiment the absorbance increases more slowly until it remains at a constant value around abs = 0.84. In the graph [Fig.30(C) this concept is even better seen: after about 15 minutes of reaction, the absorbance reaches plateau, which means that all the substrate has been hydrolysed, in fact the conversion of pNPA after the first 15 minutes is already 98%. Also in the second graph, it can be seen that the speed of hydrolysis is much greater when the reaction is catalysed by the enzyme than when it is not catalysed (in this case, the increasing absorbance is solely due to the degradation of the substrate in the test buffer). After 18 minutes, the enzyme achieved 100% conversion, whereas in the same time interval, the substrate degraded to only 5%, approximately, in the buffer.

These are reference graphs, which will be used for comparison with the catalytic properties of the synthesised nanoclusters. Their performance is obviously expected

to be lower than the enzymatic performance, but it is hoped that this will be higher than the simple degradation in the analysis buffer.

3.8.2 Kinetic analysis of catalysis by nanoclusters

Nanoclusters synthesised by exploiting the peptide ligands were tested as catalysts in the pNPA hydrolysis reaction. The kinetics of the nanoclusters were compared with each other and with a positive control given by enzymatic catalysis by P. fluorescens esterase and a negative control represented by the reaction conducted in the test buffer with the absence of catalysts.

A comparison of the catalytic efficiencies of the various systems is shown in [Fig.31], which analyses how substrate conversion varies over reaction time. The AgNC_P1 nanoclusters present the most unfavourable kinetics, in fact this is only slightly higher than the substrate degradation that would normally take place in the reaction buffer alone. With progressively higher kinetics there are the AgNC_P130%mol nanoclusters and AgNP_helices. The most promising system therefore seems to be the AgNC_P130%mol nanocluster, which, of all the systems devised, comes closest to the performance of esterase.

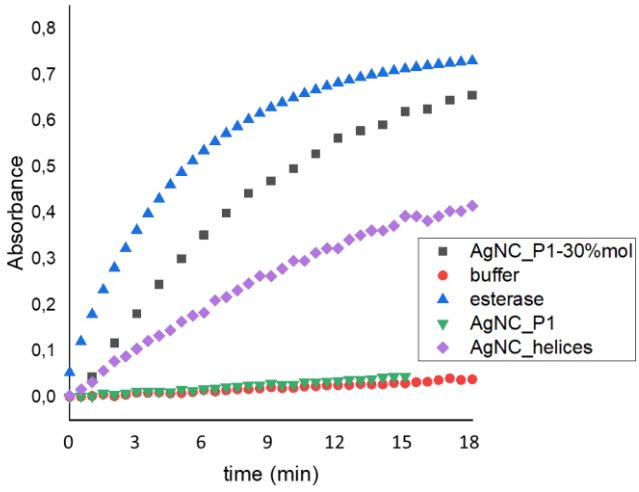

Fig.31 *Comparison of the catalytic performance of catalysts composed of silver and peptide ligands by comparing the conversion of pNPA over time.*

Measurements were performed using the catalysts at a concentration of 0.2 mg/mL, while pNPA is present at a concentration of 44 μM. For each reaction, an absorption spectrum between 380 and 420 nm is recorded every 30 seconds.

To obtain a quantitative data, the first linear section of the substrate conversion curves over time was approximated with a straight line, the slope of which indicates the initial rate of substrate hydrolysis. The values are given in [Tab.1]. The R^2 coefficient is a value that indicates how much the linear approximation fits to the starting curve that was approximated. The maximum value of R^2 is 1, indicating a perfect linear approximation, and in our case this coefficient is greater than 0.8 for each approximation, in particular, when catalysis is operated by the most promising nanoclusters, the value rises above 0.99. This allows us to make comparisons endowed with significance.

The rate of catalysis operated by the AgNC_P130%mol, which is the most interesting one, is very close to that of the enzyme, which is the target to be achieved. For all other nanoclusters, the hydrolysis rate is much lower than that of the enzyme.

catalyst	**slope**	**R^2**
AgNC_P130%mol	0,1181	0,9977
buffer	0,0015	0,3197
esterase	0,1237	0,9955
AgNC_P1	0,0032	0,6939
AgNC_helices	0,038	0,988

Tab.1 *Confronto della pendenza della curva di conversione del substrato nel tempo nel tratto lineare che va dai 0 ai 2 minuti. Il dato viene ricavato mediante l'operazione di fitting del software Origin.*

3.8.3 Cooperative effect of the nanocluster AgNC_P130%mol

Co-operativity is one of the elements that can characterise enzyme catalysis. In nature, sometimes the enzyme's previous binding to a certain molecule can positively or negatively influence the binding constant with its substrate. In the positive case, previous bond formation leads to small conformational changes in the protein, resulting in the formation of a much more optimised active site for the substrate. This increases the binding constant, so the enzyme can work faster, as it binds the substrate more quickly.

In the context of this project, cooperativity is to be identified by analysing how the rate of pNPA conversion varies when the catalyst concentration is progressively increased. The analysis involves the AgNC_P130%mol nanocluster, and it is assumed that an increase in its catalytic concentration within the reaction can lead to an increase in the conversion rate. The hypothesis is based on the possible formation of multiple catalytic sites on the surface of the nanocluster when the concentration increases, partly exploiting an aggregation effect. The aliphatic chains of the hydrophobic controllers of different nanosystems could interact with each other via hydrophobic interaction, thus leading to the agglomeration of the nanoclusters, in a manner directly proportional to the catalyst concentration in solution. Agglomeration is often something that one wants to avoid, but in this case, bringing the various systems closer together could create an even more hydrophobic environment between them, thus facilitating substrate binding and increasing the pKa of the catalytic residues. Overall, this could lead to an increase in reaction speed from a co-operative point of view, i.e. if the catalyst concentration were to double, an increase in speed would be expected, but to a greater extent than if the initial speed were to double.

Experimentally, the nanocluster is used as a catalyst in concentrations of 0.2 mg/mL, 0.4 mg/mL, 0.8 mg/mL and 1.6 mg/mL, then the concentration is doubled at each step. The absorbance curves at 400 nm over time are shown in [Fig.32], and the slope of the initial stretch from 0 to 2 minutes is shown in [Tab.2].

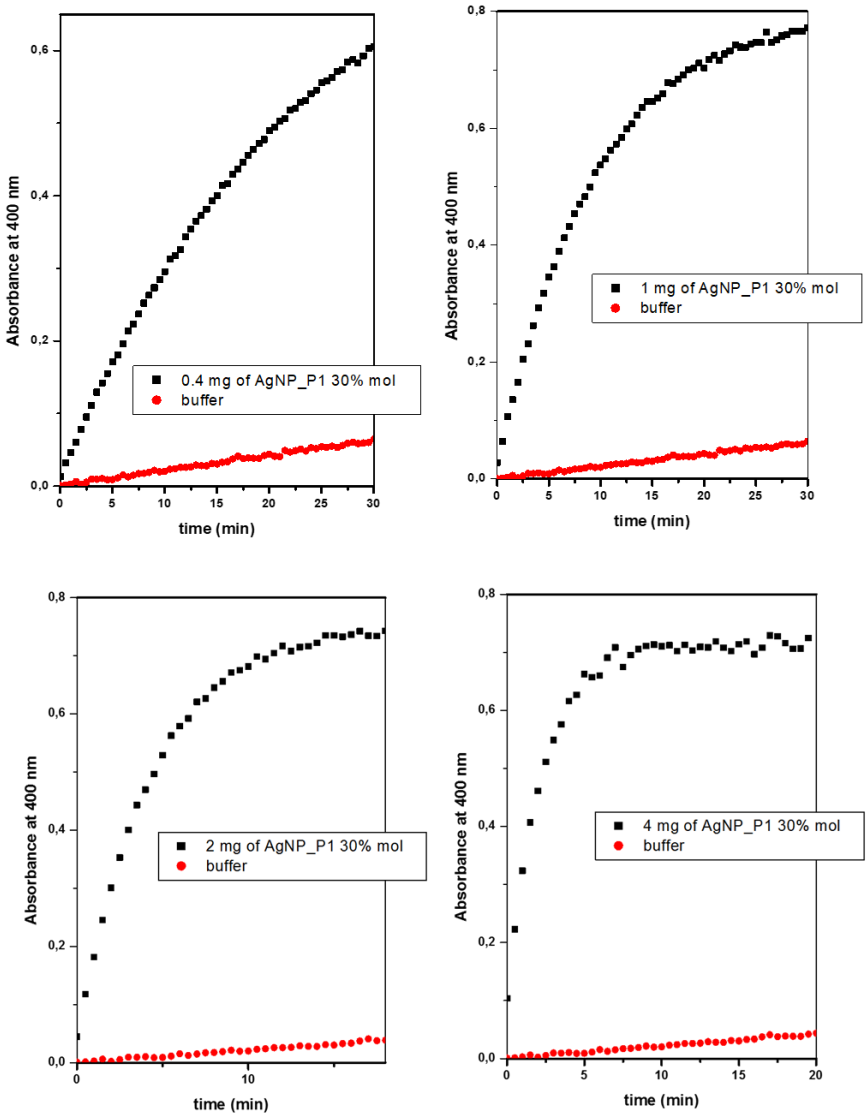

Fig.32 *Kinetic comparison of catalysis by the AgNC_P130%mol nanocluster at different catalyst concentrations. For each reaction, an absorption spectrum between 380 and 420 nm is recorded every 30 seconds. The graph shows the trend in absorbance at 400 nm as the reaction continues. The substrate is present in solution at a concentration of 39 µM.*

Concentration (mg/mL)	slope	R^2
0.2	0.031	0.997
0.4	0.069	0.994
0.8	0.128	0.998
1.6	0,180	0.981

Tab.2 *Comparison of the slope of the absorbance curve at 400 nm over time in the linear range from 0 to 2 minutes. The figure is obtained using the Origin software fitting operation.*

The R-values[2] are all greater than 0.99, so it can be considered a very good linear approximation of the first section of the curves. The initial hydrolysis rates of each sample, which can be associated with the slope of the calculated straight line, do not appear to show any presence of a cooperative effect. When the catalyst concentration doubles, the hydrolysis rate also doubles, without showing any significant increase in rate possibly brought about by cooperativity. On the contrary, when the concentration is doubled from 0.8 to 1.6 mg/mL, one would expect a slope of about 0.25, but the measured value is only 0.18. Contrary to expectations, the excessive increase in concentration could adversely affect the hydrolysis rate, possibly due to substantial agglomeration of the nanosystems. The agglomeration could be so high that it would make it more difficult for the substrate to be accommodated in the catalytic site. It is plausible that in the system that is formed, the catalytic sites on the outside of the agglomerate remain active, while those on the inside may be inactive due to the lack of pNPA binding.

3.8.4 Helices ligands

By testing various combinations and amounts of the helix ligands, it was observed that nanoclusters functionalized with a mixture of the two helices are capable of converting the sublayer. In contrast, nanoclusters that have only His-helixes or only Asp/Ser-helixes return a catalytic activity comparable to that of the buffer so we can infer that the catalytic activity of hydrolysis of the ester bond is given by the simultaneous presence of the two helices on the nanocluster surface. As the amount of nanoparticle in the cuvette increases, a higher catalytic activity can be observed [Fig.32].

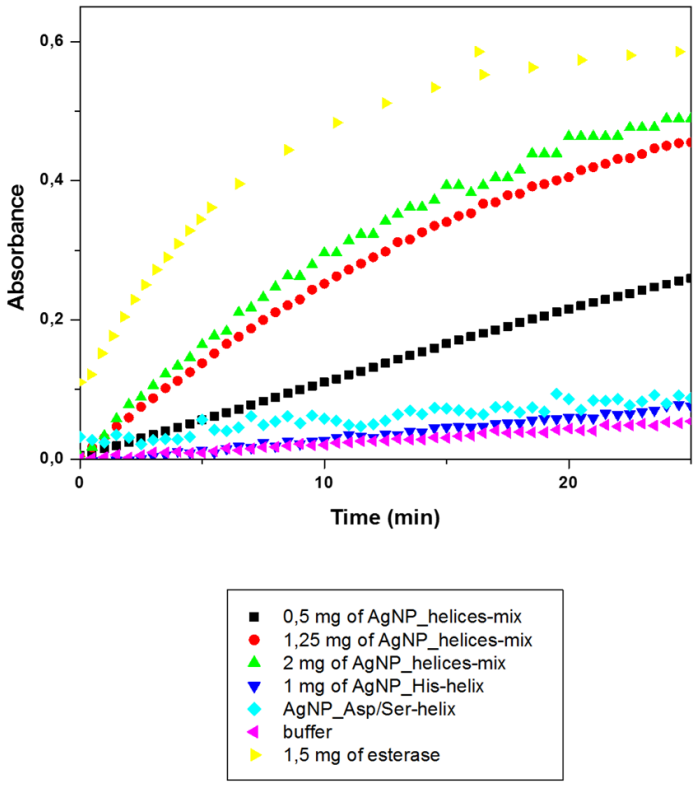

Fig.32 *Kinetic comparison of catalysis by the AgNC_helices nanoclusters at different catalyst concentrations.*

The R^2 values are all greater than 0.99, so it can be considered a very good linear appproximation of the first section of the curves. The initial hydrolysis rates of each sample, which can be associated with the slope of the calculated straight line, do not seem to show any presence of a cooperative effect. When the catalyst

concentration doubles, the hydrolysis rate also doubles, showing no significant increase in rate possibly contributed by cooperativity. Again, probably the excessive increase in concentration could adversely affect the hydrolysis rate [Tab.3].

Concentration (mg/mL)	slope	R^2
0.2	0,0093	0,9954
0.5	0,0283	0,9987
0.8	0,038	0,988

Tab.3 *Confronto della pendenza della curva di conversione del substrato nel tempo nel tratto lineare che va dai 0 ai 2 minuti. Il dato viene ricavato mediante l'operazione di fitting del software Origin.*

3.9 Characterization

3.9.1 Ligand P1

NMR analysis. The ligand P1 is characterised by NMR spectroscopy. The ^{1}H-NMR spectrum is shown in [Fig.34], where the manual peak assignment was facilitated by the analysis of the two-dimensional spectrum H-^{11}H-TOCSY [Fig.35]. The signal of the α hydrogens is either not visible or faintly visible, due to the signal suppression that has to be carried out when performing NMR measurements in D_2O. The characteristic signals of each amino acid used in the ligand synthesis can be seen very well, so that, with a certain degree of confidence, one can be sure of having the correct peptide in one's hands.

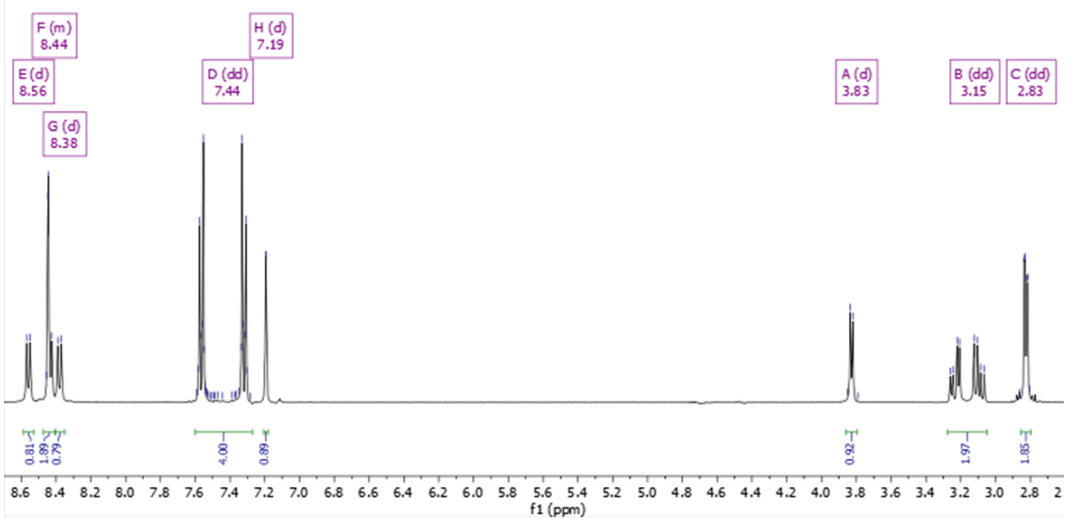

Fig.34 *1H NMR (400 MHz, H_2O + 10 % v/v D_2O) of the pMBA-SHD ligand. δ 8.56 (d, J = 7.9 Hz, His-H^N), 8.47 - 8.41 (m, Ser-H^N + His-Haromatic), 8.38 (d, J = 8.0 Hz, Asp-H^N), 7.44 (dd, pMBA-Haromatic), 7.19 (d, J = 1.4 Hz, His-Haromatic), 3.83 (d, J = 5.8 Hz, Ser-H^β), 3.15 (dd, His-H^β), 2.83 (dd, J = 6.0, 2.0 Hz, Asp-H^β).*

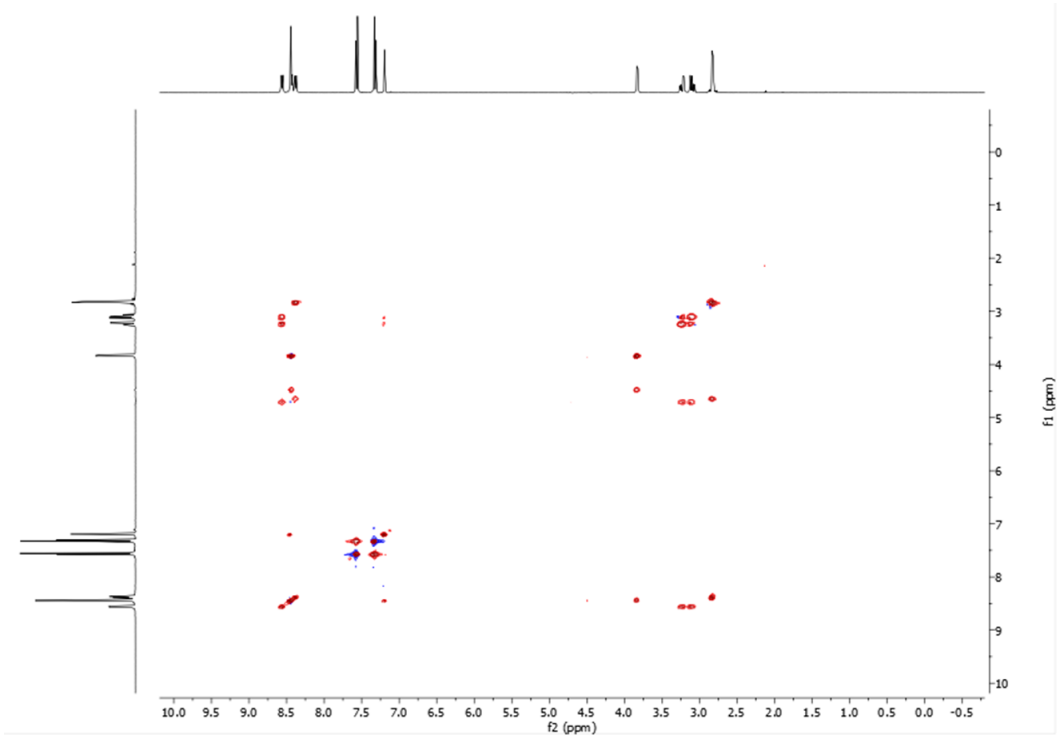

Fig.35 *Spectrum H-11 H-TOCSY (400 MHz, H_2O + 10 % v/v D_2O) of the pMBA-SHD ligand.*

3.9.2 AgNC_P1

UV-VIS absorption analysis. The fractions obtained from gel-permeation in the column were compared by analysing their UV-VIS absorption spectrum [Fig.36]. The spectrum shows two clearly recognisable peaks at around 485 and 618 nm, but absorption is also seen around 560 nm.

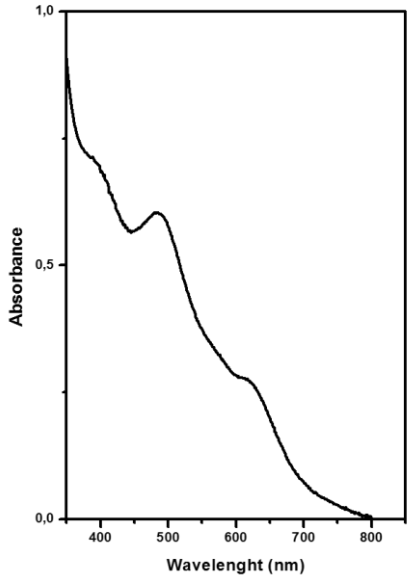

Fig.36 *UV-VIS absorption spectrum of the AgNC_P1 nanocluster.*

3.9.3 Hydrophobic controller

NMR analysis. The hydrophobic controller is characterised using NMR spectroscopy. A ^{1}H-NMR spectrum with manual peak assignment is shown in [Fig.37]. The signal of the α-hydrogen is either not visible or faintly visible, due to the signal suppression that has to be carried out when performing NMR measurements in D_2 O. The characteristic signals of each amino acid used in the ligand synthesis can be seen very well, so that with a certain degree of confidence, one can be sure of having the correct ligand in one's hands.

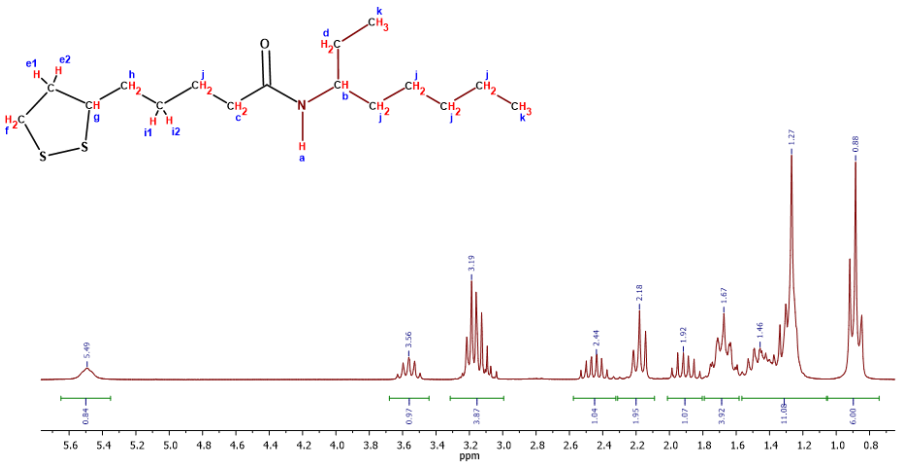

Fig.37 *^{1}H-NMR of the hydrophobic controller.*

3.9.4 AgNC_P1-30%mol

UV-VIS absorption analysis. All the fractions obtained from gel permeation in the column show the same UV-VIS absorption spectrum. This is characterised by two very broad and poorly defined absorption bands centred around 475 and 595 nm [Fig.38].

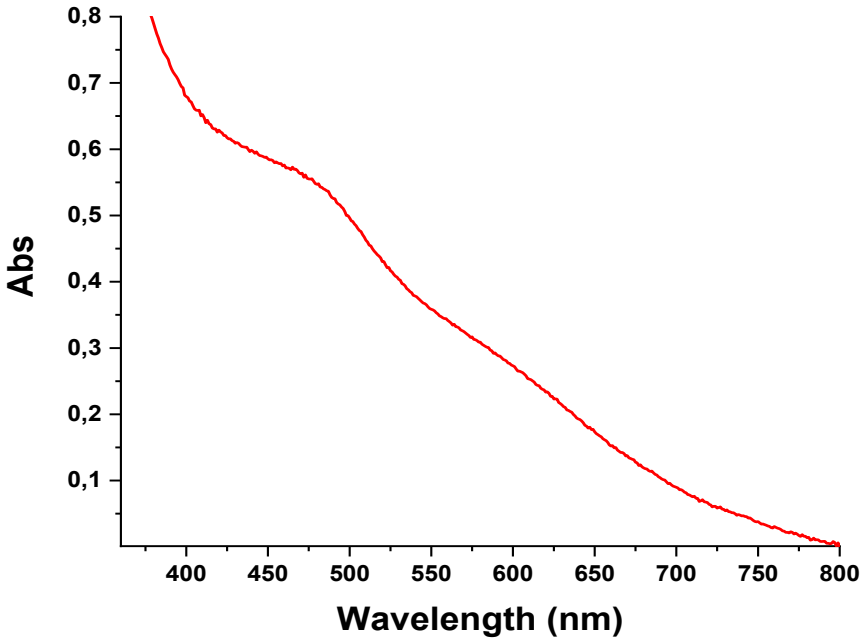

Fig.38 *UV-VIS absorption spectrum of the Ag:pMBA-SHD@30%LPAM nanocluster.*

3.9.5 His-helix ligand

The His-helix ligand is characterised by NMR spectroscopy. A ^{1}H-NMR spectrum is shown in [Fig.39,40], in which the manual assignment of peaks was facilitated by the analysis of the two-dimensional spectrum ^{1}H-^{1}H -TOCSY [Fig.41]. The characteristic signals of each amino acid used in the ligand synthesis can be discerned very well, so that, with a certain degree of confidence, one can be sure of having the correct peptide in hand. The two-dimensional spectrum ^{1}H-^{1}H-ROESY [Fig.42] allows the helical structure of the peptide to be ascertained [Fig.43].

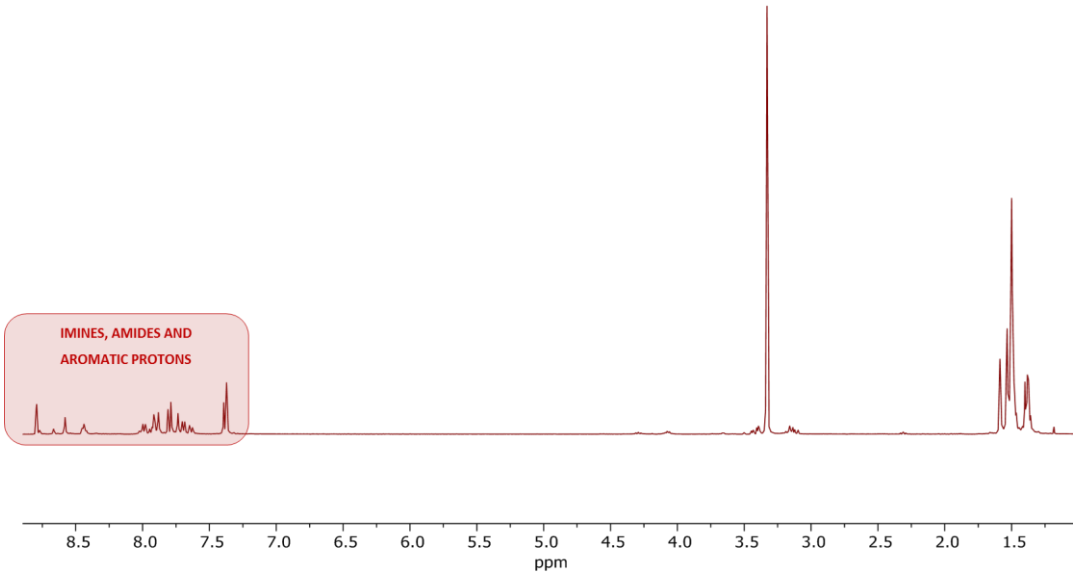

Fig.39 *Spectrum ^{1}H-NMR. The red box highlights the area with the hydrogen correlation signals of the NH amine groups of the residues present d_{NN} and the aromatic groups.*

chemical shift (ppm)	multiplet	integral	J - coupling
8.79	d	1H	J = 1.2 Hz
8.58	s	1H	
8.44	d	1H	J = 4.4 Hz
7.93	m	1H	J = 4.3 Hz
7.80	d	2H	J = 8.6 Hz
7.74	s	1H	
7.69	d	1H	J = 7.2 Hz
7.38	m	3H	

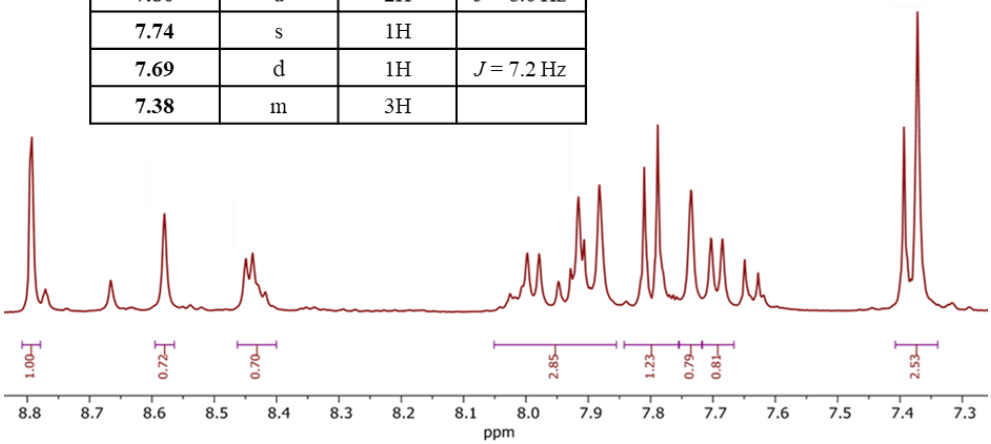

Fig.40 *Detail of the spectrum above in the area of the amine and aromatic proton signals. The chemical shifts of the identified peaks with their respective multiplicity, integral and J-coupling values are shown in the table.*

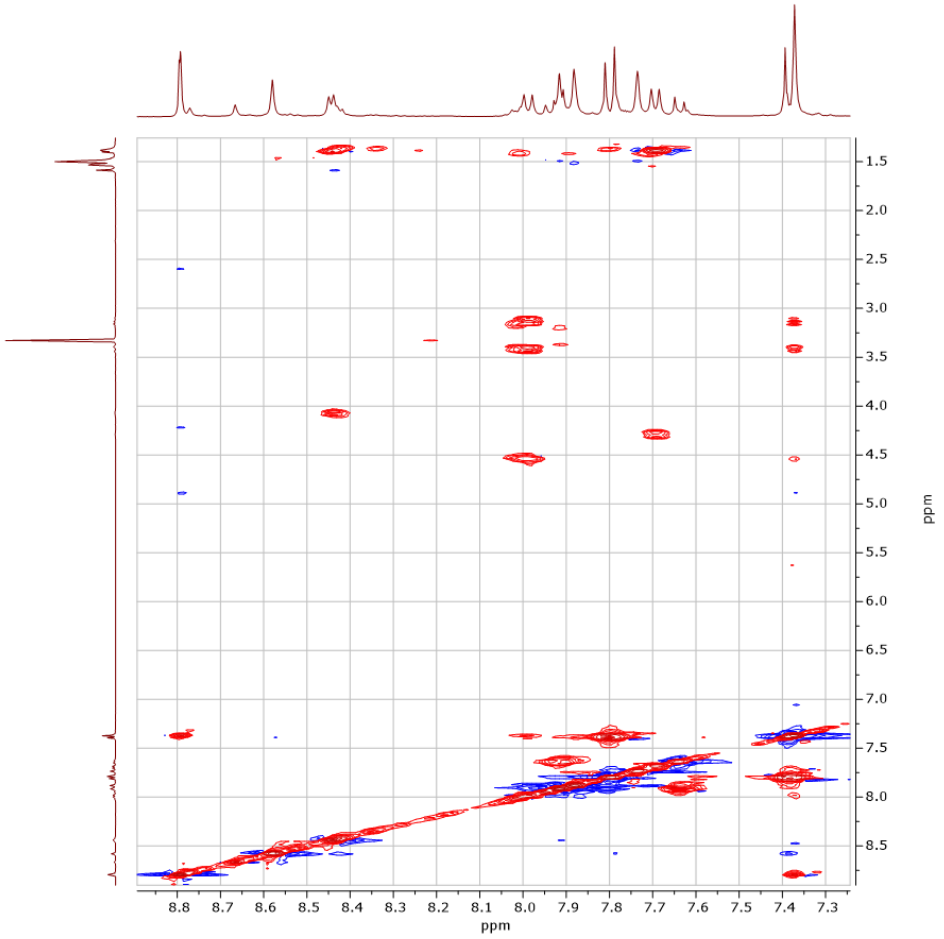

i	NH and aromatic H	αH	βH e βCH_3
pMBA	7.80, 7.38	/	/
Aib1	8.58	/	1.40, 1.50
Ala2	8.44	4.06	1.38
Aib3	7.93	/	1.40, 1.50
His	8.79, 7.93	4.52	3.41, 3.13
Aib5	7.93	/	1.40, 1.50
Ala6	7.69	4.28	1.38
Aib7	7.74	/	1.40, 1.50

Fig.41 *Detail of the spectrum ^1H-^1H-TOCSY with NH and aromatic signals. The table shows the chemical shifts of the coupling signals d_{NN} and on the side chain of the residues ($d_{\alpha N}$ $d_{N\beta N}$), which allow the residues of the His-helix peptide sequence to be identified.*

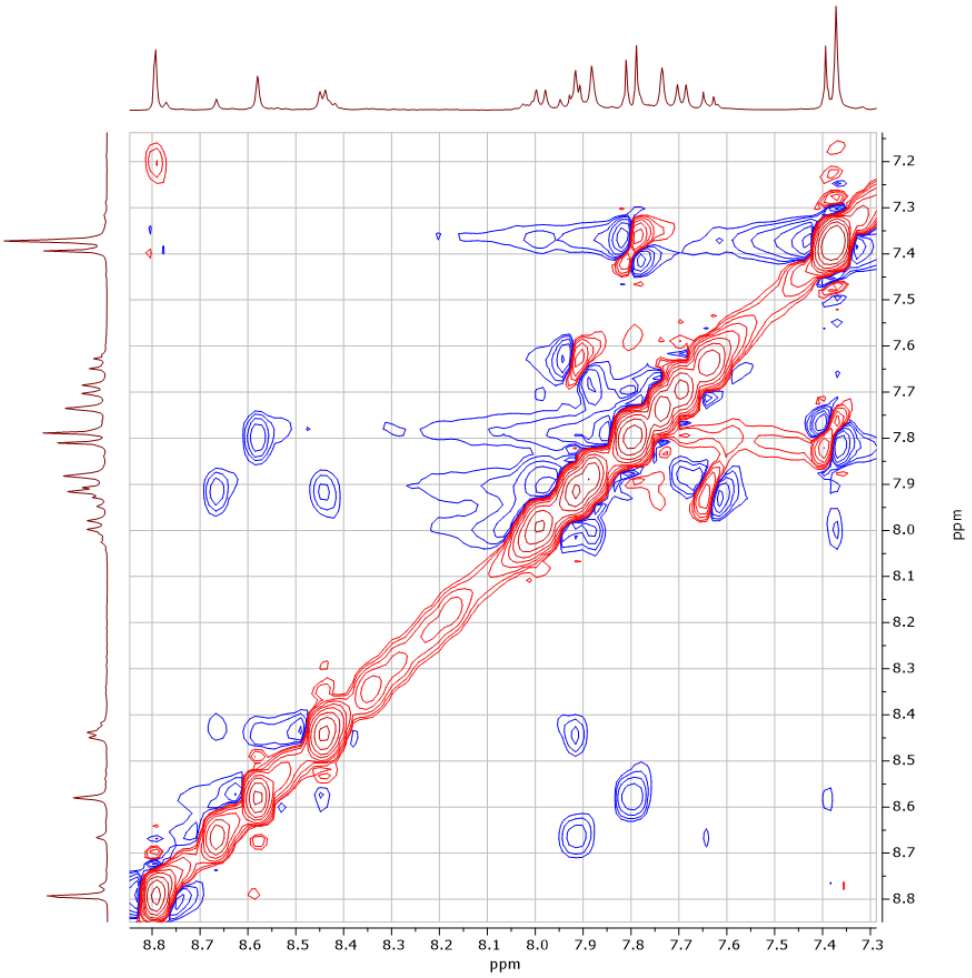

i	d_{NN} (i, i+1)	d_{NN} (i, i+3)
pMBA	Aib1	Aib3
Aib1	pMBA, Ala2	His
Ala2	Aib1	Aib5
Aib3	His	pMBA
His	Aib3, Aib5	Aib1
Aib5	His, Ala6	Ala2
Ala6	Aib5, Aib7	

Fig.42 *Detail of the spectrum ^{1}H-^{1}H-ROESY with NH and aromatic signals. The table shows the couplings between contiguous dNN residues (i, i+1) confirming the sequence of the identified residues. Couplings between residues spaced three residues apart are also shown, confirming the assumed helical secondary structure.*

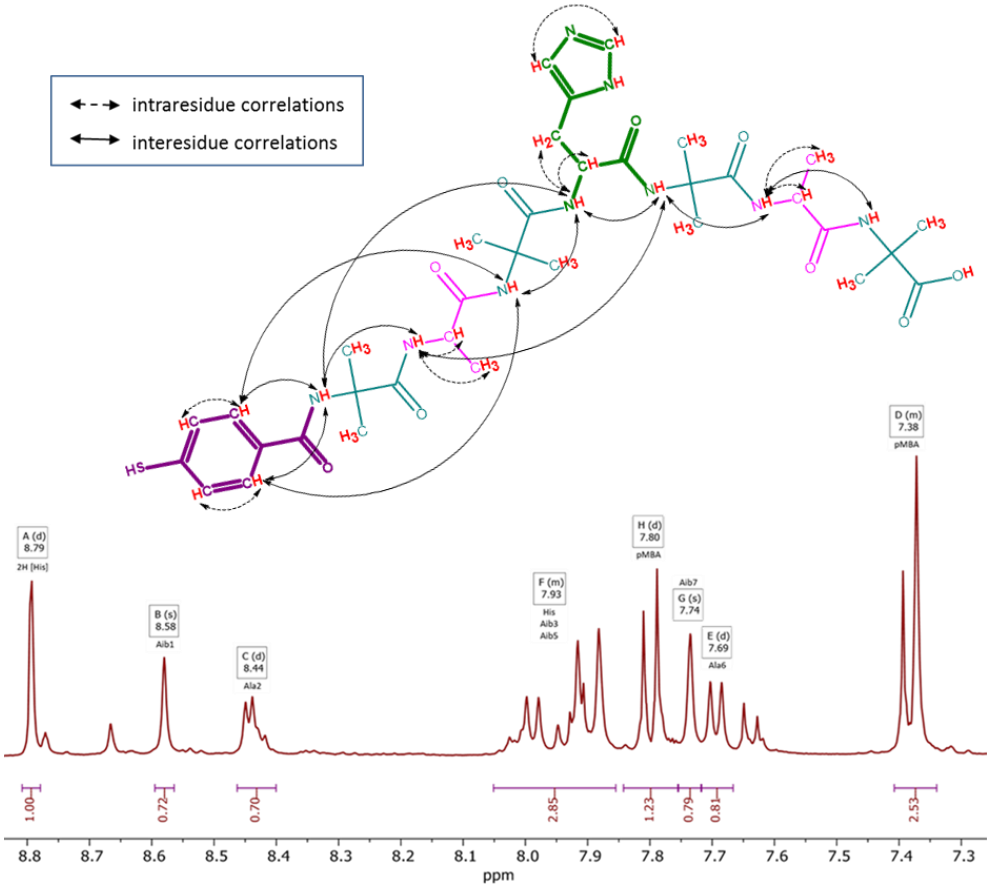

Fig.43 *The image shows the sequence of the peptide with the various identified couplings highlighted by arrows. Also shown is the detail of the area* ^{1}*H-NMR with the assignments of the amine and aromatic signals to the respective residues.*

Analysis of circular dichroism. Two negative absorption bands stand out in the circular dichroism spectrum of the His-helix [Fig.44]. One is at 225 nm, which is typical of the interaction between the amide group (peptide bond) and the amino acid residues in the helical structure. The other band is found at 200 nm in the near UV, which is often indicative of a well-formed α-helical structure. The latter type of band results from the geometry of the peptide bond and the interactions between the hydrogen atoms along the helix and at 225 nm. In contrast, a positive band is present at around 275 nm due to the absorbance of the aromatic pMBA structure present in the peptide.

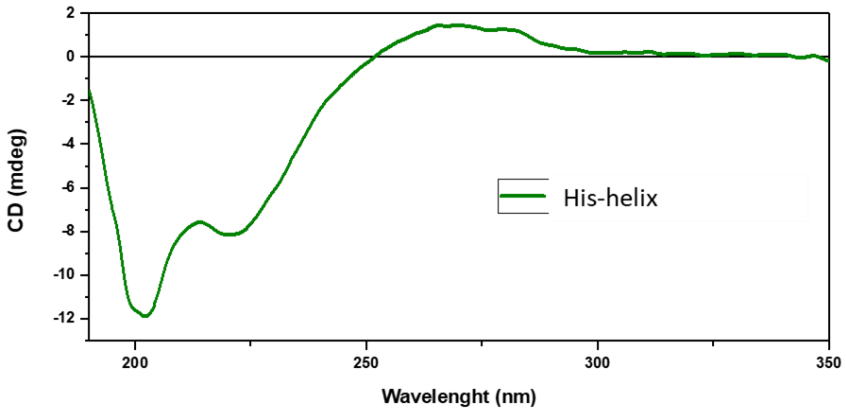

Fig.44 *Circular dichroism spectrum of His-helix.*

The circular dichroism performed on the His-helix functionalized nanoclusters has the same pattern as the same free helix in solution so it can be assumed that the helical structure is maintained even after functionalization [Fig.45].

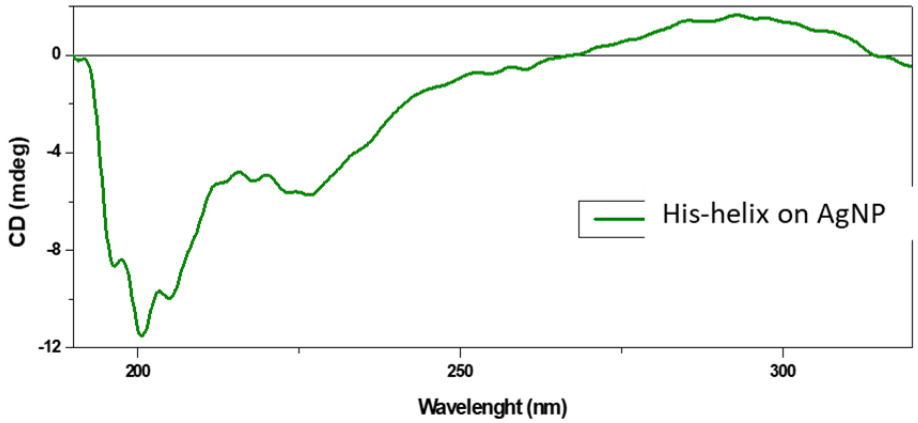

Fig.45 *Circular dichroism spectrum of AgNC_His-helix*

3.9.6 Asp/Ser-helix ligand

The Asp/Ser-helix ligand is characterised by NMR spectroscopy. A ^{1}H-NMR spectrum is shown in [Fig.46,47], in which the manual assignment of peaks was facilitated by the analysis of the two-dimensional spectrum ^{1}H-^{1}H-TOCSY [Fig.48]. The characteristic signals of each amino acid used in the ligand synthesis can be discerned very well, so that, with a certain degree of confidence, one can be sure of having the correct peptide in hand. The two-dimensional spectrum H-^{11} H-

ROESY [Fig.49] allows the helical structure of the peptide to be ascertained [Fig.50].

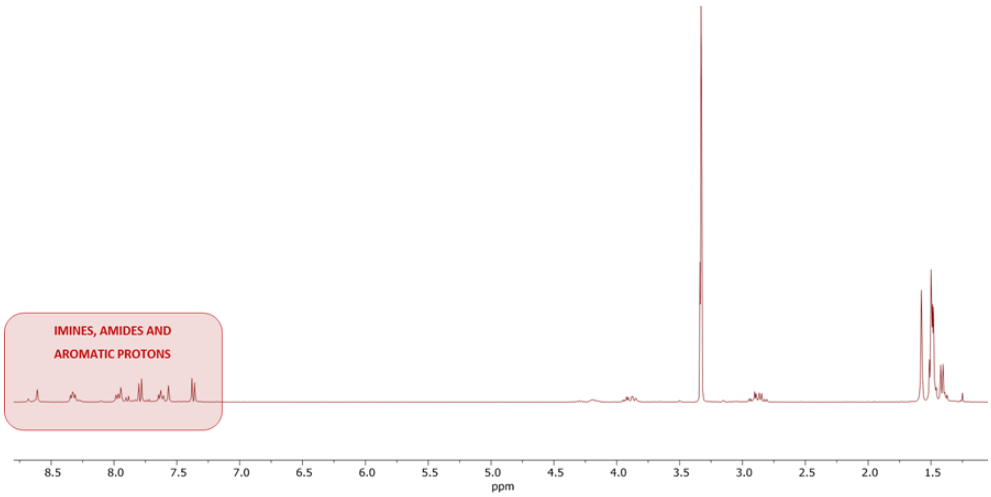

Fig.46 *Spectrum [1] H-NMR. The red box highlights the area with the hydrogen correlation signals of the NH amine groups of the residues present* d_{NN} *and the aromatic groups.*

chemical shift (ppm)	multiplet	integral	J - coupling
8.61	s	1H	
8.38 – 8.29	m	4H	
8.27	d	1H	J = 6.9 Hz
8.02 – 7.92	m	4H	
7.89	d	1H	J = 8.6 Hz
7.73	d	1H	J = 8.6 Hz
7.63	t	3H	J = 8.0 Hz
7.57	s	1H	
7.37	d	2H	J = 8.7 Hz

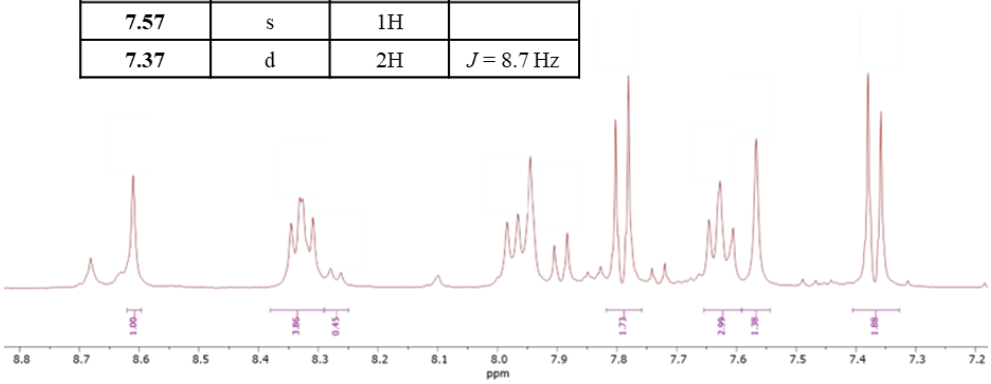

Fig.47 *Detail of the spectrum above in the area of the amine and aromatic proton signals. The chemical shifts of the identified peaks with their respective multiplicity, integral and J-coupling values are shown in the table.*

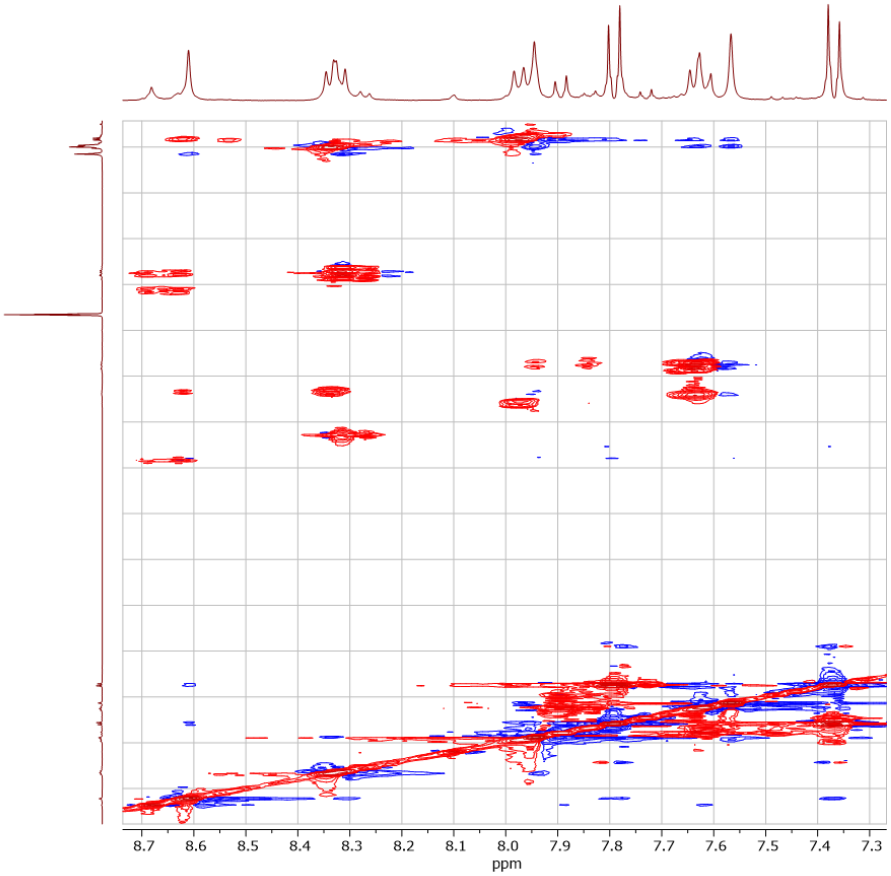

	chemical shift (ppm)		
i	**NH and aromatic H**	**αH**	**βH e βCH_3**
pMBA	7.79, 7.37	/	/
Aib1	8.61	/	1.40, 1.55
Asp	8.27	4.65	2.95, 2.80
Ala3	8.33	4.20	1.40
Aib4	7.89	/	1.40, 1.50
Ser	7.63	4.18	3.95, 3.90
Ala6	7.97	4.30	1.33
Aib7	7.57	/	1.40, 1.50

Fig.48 *Detail of the spectrum ^{1}H-^{1}H-TOCSY with NH and aromatic signals. The table shows the chemical shifts of the coupling signals d_{NN} and on the side chain of the residues ($d_{\alpha N}$ $d_{N\beta N}$), which allow the residues of the Asp/Ser-helix peptide sequence to be identified.*

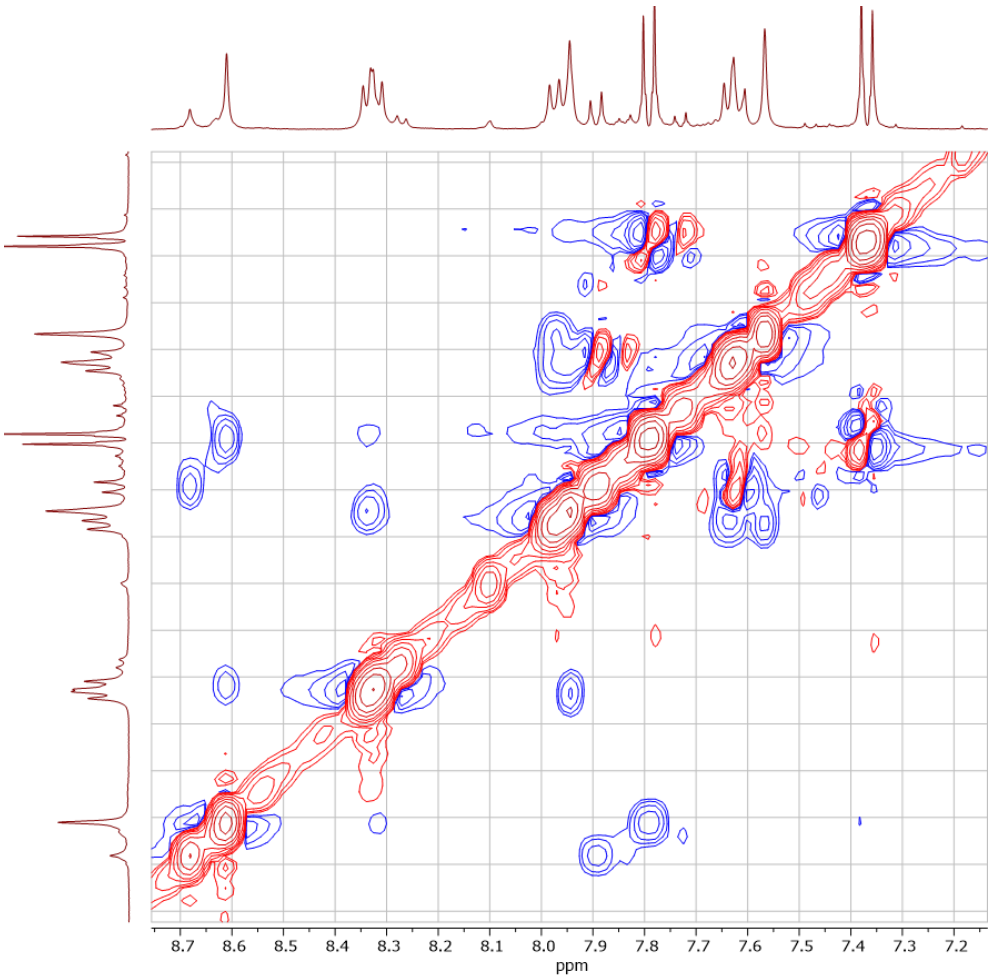

i	d_{NN} (i, i+1)	d_{NN} (i, i+3)
pMBA	Aib1	Ala3
Aib1	pMBA, Asp	Aib4
Asp	Aib1, Ala3	
Ala3	Asp	pMBA; Ala6
Aib4	Ser	Aib1
Ser	Aib4, Ala6	
Ala6	Ser, Aib7	Ala3

Fig.49 *Detail of the spectrum ^{1}H-^{1}H-ROESY with NH and aromatic signals. The table shows the couplings between contiguous dNN residues (i, i+1) confirming the sequence of the identified residues. Couplings between residues spaced three residues apart are also shown, confirming the assumed helical secondary structure.*

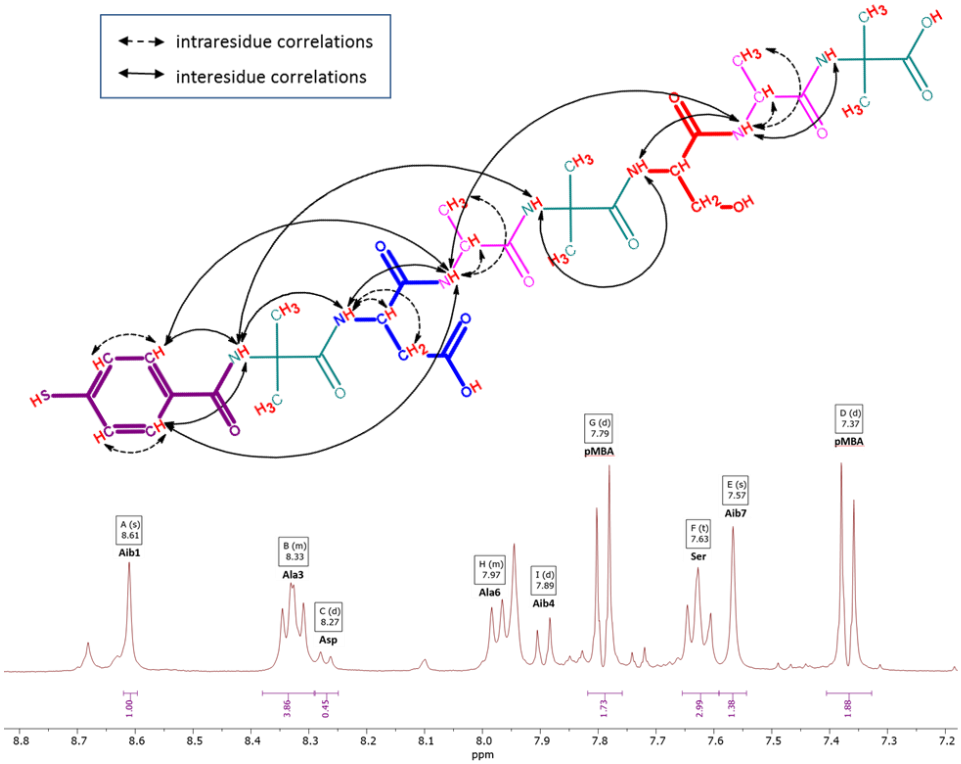

Fig.50 *The image shows the sequence of the peptide with the various identified couplings highlighted by arrows. Also shown is the detail of the are a ^{1}H-NMR with the assignments of the amine and aromatic signals to the respective residues.*

Circular dichroism. Two negative absorption bands stand out in the circular dichroism spectrum of the His-helix [Fig.51]. One is at 225 nm, which is typical of the interaction between the amide group (peptide bond) and the amino acid residues in the helical structure. The other band is found at 200 nm in the near UV, which is often indicative of a well-formed α-helical structure. The latter type of band results from the geometry of the peptide bond and the interactions between the hydrogen atoms along the helix and at 225 nm. In contrast, a positive band is present at around 275 nm due to the absorbance of the aromatic pMBA structure present in the peptide.

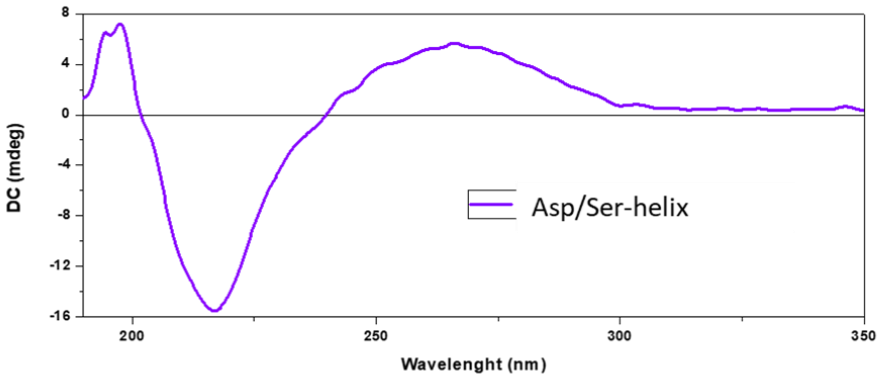

Fig.51 *Circular dichroism spectrum of Asp/Ser-helix.*

The circular dichroism performed on the Asp/Ser-helix functionalized nanoclusters has the same pattern as the same free helix in solution so it can be assumed that the helical structure is maintained even after functionalization [Fig.52].

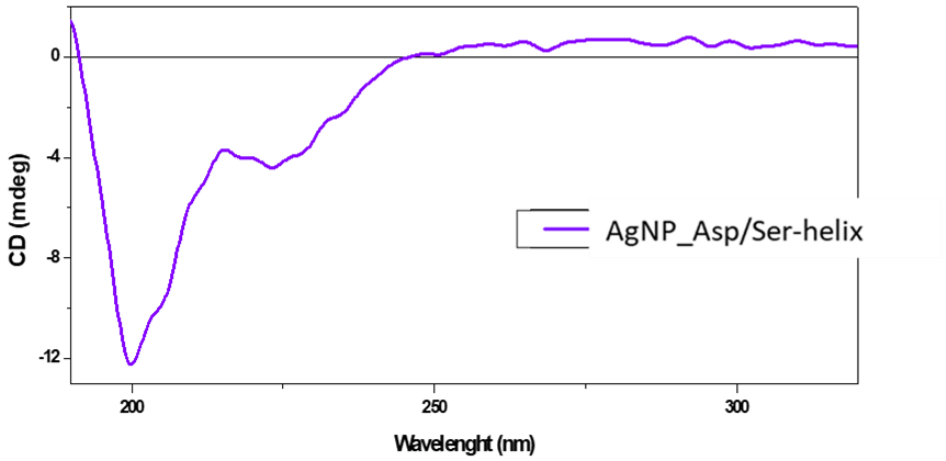

Fig.52 *Circular dichroism spectrum of AgNC_Asp/Ser-helix.*

4. CONCLUSIONI

Biomimicry is a field of research in which various scientific groups spend their strengths and resources. By analyzing the structure of biological macromolecules, one realizes that their composition is given by the assembly of a small number of small molecules. As is well known, the variety of molecular macrosystems that exist is given not only by the nature of the constituent elements, but also by their relative and precise spatial arrangement. Among proteins, enzymes have been selected for their catalytic properties toward specific chemical reactions, assuming an essential role in the biological system in which they operate. Under physiological conditions, enzymatic hydrolytic catalysis is much more efficient than homogeneous or heterogeneous chemical catalysis; in addition, enzymes are endowed with greater selectivity. The beating heart of enzymatic hydrolytic catalysis is the catalytic triad, which is the set of three highly conserved amino acids (aspartate, serine and histidine) that cooperate within the enzymatic catalytic site to catalyze a specific reaction. In this study, we sought to reproduce an environment that mimicked the enzyme catalytic pocket by the formation of a peptide monolayer on the surface of a silver nanocluster. The pMBA was functionalized on the N-terminal portion of short peptide sequences consisting of the residues of the catalytic triad. Initial functionalization tests were conducted with small noncatalytic model peptides, exploiting pre- and post-synthesis functionalization methodologies of nanoclusters. Subsequently, catalytic peptide ligands were synthesized by solid-phase peptide synthesis, and once purified were used in the formation of silver nanoclusters. Different catalytic ligands have been devised that differ in the spatial arrangement of the residues and the strategy used to recreate a hydrophobic environment next to the catalytic site, which is essential to have optimal residue pKa to induce a hydrolytic process. The catalytic properties of the synthesized nanosystems were tested on the hydrolysis reaction of paranitrophenylacetate in PBS (pH=7.8), comparing their performance with that of Pseudomonas fluorescens esterase. Comparison of the performance of substrate conversion over time and the initial rate of hydrolysis shows that the most promising nanocluster, and the one

that comes closest to the performance of an enzyme is the one composed of AgNC_P130%mol. The synthesized nanoclusters were characterized by UV-VIS spectroscopy and circular dichroism, while the peptide ligands were analyzed by NMR. In conclusion, in the present study, the feasibility of recreating the enzyme catalytic site on the surface of silver nanoclusters was demonstrated by exploiting the self-assembly of small peptides that can coordinate to silver. By varying the spatial arrangement of the catalytic residues and the type of hydrophobic residues present in the ligand sequence, it will be possible to aim at obtaining a higher catalytic capacity, hopefully as similar as possible to the enzymatic one.

5. BIBLIOGRAPHY

1) Bayda S. *et al*. The History of Nanoscience and Nanotechnology: From Chemical–Physical Applications to Nanomedicine. Molecules, 25(1), 112. doi:10.3390/molecules25010112
2) Rambaran T. *et al.* Nanotechnology from lab to industry - a look at current trends. Nanoscale Adv. 2022 Aug 1;4(18):3664-3675. doi: 10.1039/d2na00439a
3) Gao Y. *et al*. China and the United States--Global partners, competitors and collaborators in nanotechnology development. Nanomedicine. 2016 Jan;12(1):13-9. doi: 10.1016/j.nano.2015.09.007
4) Zhou, J., Chizhik, A.I., Chu, S. *et al.* Single-particle spectroscopy for functional nanomaterials. *Nature* **579**, 41–50 (2020). doi:10.1038/s41586-020-2048-8
5) Hao, E., Schatz, G.C. & Hupp, J.T. Synthesis and Optical Properties of Anisotropic Metal Nanoparticles. *Journal of Fluorescence* **14**, 331–341 (2004). doi:10.1023/B:JOFL.0000031815.71450.74
6) Zhang, J.Z., Noguez, C. Plasmonic Optical Properties and Applications of Metal Nanostructures. *Plasmonics* **3**, 127–150 (2008). doi:10.1007/s11468-008-9066-y
7) Vincenzo Amendola *et al* 2017 *J. Phys.: Condens. Matter* **29** 203002**DOI** 10.1088/1361-648X/aa60f3
8) Ndolomingo, M.J., Bingwa, N. & Meijboom, R. Review of supported metal nanoparticles: synthesis methodologies, advantages and application as catalysts. *J Mater Sci* **55**, 6195–6241 (2020). doi:10.1007/s10853-020-04415-x
9) van Deelen, T.W., Hernández Mejía, C. & de Jong, K.P. Control of metal-support interactions in heterogeneous catalysts to enhance activity and selectivity. *Nat Catal* **2**, 955–970 (2019). doi:10.1038/s41929-019-0364-x
10) Ansar, S., Tabassum, H., Aladwan, N.S.M. *et al.* Eco friendly silver nanoparticles synthesis by *Brassica oleracea* and its antibacterial, anticancer and antioxidant properties. *Sci Rep* **10**, 18564 (2020). https://doi.org/10.1038/s41598-020-74371-8

11) Ullah Khan S. et al. Nanosilver: new ageless and versatile biomedical therapeutic scaffold. Int J Nanomedicine. 2018 Feb 2;13:733-762. doi: 10.2147/IJN.S153167
12) Prosposito P. *et al*. Silver Nanoparticles as Colorimetric Sensors for Water Pollutants. Chemosensors. 8. 26. doi:10.3390/chemosensors8020026.
13) UV/VIS/IR Spectroscopy Analysis of Nanoparticles, 2012. [(accessed on 5 March 2016)].
14) Huang T. *et al*. Synthesis and Characterization of Tunable Rainbow Colored Colloidal Silver Nanoparticles Using Single-Nanoparticle Plasmonic Microscopy and Spectroscopy. J Mater Chem. 2010 Jan 1;20(44):9867-9876. doi: 10.1039/C0JM01990A
15) Pérez-Tanoira R. *et al*. Silver Nanoparticles Produced by Laser Ablation and Re-Irradiation Are Effective Preventing Peri-Implantitis Multispecies Biofilm Formation. Int J Mol Sci. 2022 Oct 10;23(19):12027. doi: 10.3390/ijms231912027
16) Behera A. *et al*. Magnetron sputtering for development of nanostructured materials. Design, Fabrication, and Characterization of Multifunctional Nanomaterials. 2022;177-199. doi:10.1016/B978-0-12-820558-7.00002-9
17) Yusuf M. Silver Nanoparticles: Synthesis and Applications. Handbook of Ecomaterials. 2018 Nov 30:2343–56. doi: 10.1007/978-3-319-68255-6_16. PMCID: PMC7122521.
18) Roldán MV. *et al*. "Electrochemical Method for Ag-PEG Nanoparticles Synthesis", Journal of Nanoparticles, vol. 2013, Article ID 524150, 7 pages, 2013. doi: 10.1155/2013/524150
19) Al-Zahrani S. *et al*. Role of Synthetic Plant Extracts on the Production of Silver-Derived Nanoparticles. Plants (Basel). 2021 Aug 13;10(8):1671. doi: 10.3390/plants10081671
20) Kalishwaralal K. *et al*. Extracellular biosynthesis of silver nanoparticles by the culture supernatant of Bacillus licheniformis, Materials Letters, Volume 62, Issue 29, 2008, Pages 4411-4413, ISSN 0167-577X. doi: 10.1016/j.matlet.2008.06.051
21) Kang X. *et al*. $Au_{25}(SR)_{18}$: the captain of the great nanocluster ship. Nanoscale, 10(23), 10758–10834. doi:10.1039/c8nr02973c

22) Shen H. *et al*. N-Heterocyclic Carbene-Stabilized Gold Nanoclusters with Organometallic Motifs for Promoting Catalysis. Journal of the American Chemical Society 2022 144 (24), 10844-10853. doi: 10.1021/jacs.2c02669

23) Desireddy A. *et al*. Ultrastable silver nanoparticles. Nature 501, 399–402 (2013). doi: 10.1038/nature12523

24) Apostolopoulos V. *et al*. A Global Review on Short Peptides: Frontiers and Perspectives. Molecules. 2021 Jan 15;26(2):430. doi: 10.3390/molecules26020430

25) Bakr OM. *Et al*. Silver nanoparticles with broad multiband linear optical absorption. Angew Chem Int Ed Engl. 2009;48(32):5921-6. doi: 10.1002/anie.200900298

26) Khalkho BR. *et al*. Citrate functionalized gold nanoparticles assisted micro extraction of L-cysteine in milk and water samples using Fourier transform infrared spectroscopy, Spectrochimica Acta Part A: Molecular and Biomolecular Spectroscopy, Volume 267, Part 2, 2022, 120523, ISSN 1386-1425. doi: 10.10167j.saa.2021.120523

27) Spears RJ. *et al*. Cysteine protecting groups: applications in peptide and protein science. Chemical Society Reviews 2021,**50**, 11098-11155. doi: 10.1039/D1CS00271F

28) Neelam Gurung, Sumanta Ray, Sutapa Bose, Vivek Rai, "A Broader View: Microbial Enzymes and Their Relevance in Industries, Medicine, and Beyond", BioMed Research International, vol. 2013, Article ID 329121, 18 pages, 2013. https://doi.org/10.1155/2013/329121Agnihotri S. et al. RSC Adv., 2014, 4 , 3974. doi: 10.1039/C3RA44507K

29) Divya Sharma, Kamal Kumar Bhardwaj & Reena Gupta (2022) Immobilization and applications of esterases, Biocatalysis and Biotransformation, 40:3, 153-168, DOI: 10.1080/10242422.2021.2013825

30) Nanda, V., Koder, R. Designing artificial enzymes by intuition and computation. *Nature Chem* **2**, 15–24 (2010). https://doi.org/10.1038/nchem.473

31) Nicolae-Maranciuc A. *et al*. Ag Nanoparticles for Biomedical Applications-Synthesis and Characterization-A Review. Int J Mol Sci. 2022 May 21;23(10):5778. doi: 10.3390/ijms23105778

32) Pingali KC. *et al*. Silver Nanoparticles from Ultrasonic Spray Pyrolysis of Aqueous Silver Nitrate, Aerosol Science and Technology, 39:10, 1010-1014. doi: 10.1080/02786820500380255

33) Loiseau A. *et al*. Silver-Based Plasmonic Nanoparticles for and Their Use in Biosensing. Biosensors (Basel). 2019 Jun 10;9(2):78. doi: 10.3390/bios9020078

34) Xu L. *et al*. Silver nanoparticles: Synthesis, medical applications and biosafety. Theranostics. 2020 Jul 11;10(20):8996-9031. doi: 10.7150/thno.45413

35) Akintayo DC. et al. Practical Peptide Synthesis Workflow Using Amino-Li-Resin. *MethodsProtoc.*2022,*5*,72. doi: 10.3390/mps5050072

36) Wang L. *et al*. Therapeutic peptides: current applications and future directions. Signal Transduct Target Ther. 2022 Feb 14;7(1):48. doi: 10.1038/s41392-022-00904-4

37) Kumar S. *et al*. Glutathione-stabilized magic-number silver cluster compounds. Am. Chem. Soc. 2010, 132, 13141. doi: 10.1021/ja105836b

38) Zhang XF. *et al*. Silver Nanoparticles: Synthesis, Characterization, Properties, Applications, and Therapeutic Approaches. Int J Mol Sci. 2016 Sep 13;17(9):1534. doi: 10.3390/ijms17091534

39) Huang T. *et al*. Synthesis and Characterization of Tunable Rainbow Colored Colloidal Silver Nanoparticles Using Single-Nanoparticle Plasmonic Microscopy and Spectroscopy. J Mater Chem. 2010 Jan 1;20(44):9867-9876. doi: 10.1039/C0JM01990A

40) Helferich B. *et al*. Trityl Ethers of Carbohydrates, Editor(s): W.W. Pigman, M.L. Wolfrom, Stanley Peat, Advances in Carbohydrate Chemistry, Academic Press, Volume 3, 1948, Pages 79-111, ISSN 0096-5332, ISBN 9780120072033. doi: 10.1016/S0096-5332(08)60027-2

41) Spears RJ. *et al*. Cysteine protecting groups: applications in peptide and protein science. Chemical Society Reviews 2021,**50**, 11098-11155. doi: 10.1039/D1CS00271F